International Journal of Thermophysics _####################_
https://doi.org/10.1007/s10765-025-03616-3

Thermophysical Analysis and Molecular Modeling of 2-Propanol–Glycol Ether Mixtures Between 293.15 K and 323.15 K: Implications for Renewable Fuel Formulations

Khaoula Samadi[1,4] · Mohamed Lifi[2] · Ilham Abala[3] · Natalia Muñoz-Rujas[4] · Fatima Ezzahrae M'hamdi Alaoui[1] · Fernando Aguilar[4]

Received: 7 July 2025 / Accepted: 21 July 2025

Abstract

Short-chain alcohols and glycol ethers are increasingly being considered as promising additives or components in biofuels due to their favorable physicochemical properties and alignment with the growing demand for sustainable and low-emission energy sources in the transportation sector. This study presents experimental data for five binary mixtures of 2-propanol with glycol ethers: 2-(2-methoxyethoxy)ethanol, 2-(2-ethoxyethoxy)ethanol, 2-methoxyethanol, 2-phenoxyethanol, and 2-butoxyethanol. Measurements of excess molar enthalpy (H_m^E), density (ρ), speed of sound (u), and refractive index (n_D) were performed over the temperature range 293.15 K–323.15 K at 0.1 MPa. Derivative thermodynamic properties, excess molar volume (V^E), isentropic compressibility (k_s), and refractive index deviation (Δn_D), were calculated from the experimental data. Density data were correlated using PC-SAFT and Peng–Robinson equations of state, while polynomial equations were employed to fit ρ, u, n_D, and k_s as functions of composition. The Redlich–Kister equation was used to fit V^E and Δn_D. Excess molar enthalpy (H_m^E) was modeled using both the Redlich–Kister correlation and thermodynamic activity coefficient models, UNIQUAC, NRTL, and Modified UNIFAC, to interpret molecular interactions. All the studied mixtures exhibit endothermic behavior. The results contribute to a deeper understanding of the behavior of alcohol/glycol ether mixtures and their potential application in fuel formulations.

Keywords 2-propanol · Glycol ethers · Local composition models · PC-SAFT EoS · Peng–Robinson EoS · Redlich–Kister correlation · Renewable energy

Extended author information available on the last page of the article

1 Introduction

The transition to renewable energy has become a global imperative, particularly in the transportation sector, which remains one of the largest contributors to greenhouse gas emissions. Reducing the environmental impact of transport fuels is crucial to meeting climate targets and promoting sustainable development [1]. Consequently, biomass derived alternative fuels are attracting significant interest as they offer a renewable source and a reduced ecological footprint compared to conventional options [2].

Biomass derived oxygenated solvents offer potential for cleaner fuel formulations [3]. Combining ether and hydroxyl functionalities in their structure enables potent interactions (hydrogen bonding, dipole–dipole) with alcohols such as 2-PrOH [4]. 2-PrOH, a secondary alcohol with favorable blending characteristics, is widely studied for its potential role in biofuel formulations due to its solubility, volatility, and combustion performance [5]. Its oxygen content helps promote cleaner combustion by facilitating the oxidation of hydrocarbons, leading to a reduction in carbon monoxide, unburned hydrocarbons, and particulate emissions [6]. Additionally, 2-PrOH improves the cold-start behavior of engines and enhances atomization due to its surface tension-lowering effect, which contributes to more efficient fuel–air mixing. As a molecule derived from renewable resources through fermentation processes, it aligns with green chemistry principles and offers a sustainable alternative to fossil-derived additives [7].

A great deal of potential has been demonstrated by binary mixtures of 2-PrOH with various biomass-derived glycol ethers in enhancing alternative fuel formulations. These include 22MEE, 22EEE, 2ME, 2PhE and 2BE. Each of these oxygenated compounds offers specific advantages to the blend. 22MEE has a high boiling point and low volatility, which makes it effective at limiting evaporative emissions and improving the fuel's thermal stability [8]. Conversely, 22EEE has a slightly more hydrophobic nature, favouring better integration with hydrocarbon based components and contributing to more uniform combustion [9, 10]. The more volatile 2ME offers a higher oxygen content, enhancing combustion efficiency and facilitating engine start-up at lower temperatures [11, 12]. 2PhE, which is distinguished by its aromatic ring, increases fuel density and decreases volatility [13, 14]. This reduces evaporation losses and improves the solubilisation of nonpolar fuel constituents. Lastly, 2BE strikes a favourable balance between hydrophilic and hydrophobic interactions [15].

Industrial research increasingly targets sustainable energy solutions, emphasizing the importance of thermodynamics in selecting low-impact systems. A key aspect of this effort involves studying thermophysical properties such as density, speed of sound, refractive index, and excess molar enthalpy. These properties provide valuable insights into molecular interactions, phase behavior, and the structural organization of fluid mixtures, which are crucial for designing and optimizing efficient energy systems [16]. Excess molar enthalpy reflects the deviation from ideal mixing behavior and serves as a direct indicator of intermolecular interactions within mixtures [17]. When combined with other measurable

properties, it helps deepen the understanding of system energetics and compatibility of components. Experimental determination of these properties not only supports the characterization of new substances but also provides a solid foundation for the calibration and validation of thermodynamic models. Once validated, these models enable the prediction of system behavior under a wide range of conditions, significantly reducing the need for extensive experimentation.

In the present study, we report experimental measurements for a series of binary mixtures consisting of 22MEE (1) + 2-PrOH (2); 22EEEl (1) + 2-PrOH (2); 2ME (1) + 2-PrOH (2); 2PhE (1) + 2-PrOH (2) and 2BE (1) + 2-PrOH (2), over a temperature range from 293.15 K to 323.15 K and at a pressure of 0.1 MPa. The investigated properties include excess molar enthalpy (H_m^E), density (ρ), speed of sound (u), and refractive index (n_D). From these properties, several derivative properties were calculated, such as excess molar volume (V^E), isothermal compressibility (k_s), and deviation in refractive index (Δn_D). The H_m^E was determined using a quasi-isothermal flow calorimeter; The ρ *and* u were obtained using an Anton Paar DSA 5000 M densitometer, while the n_D was measured using a digital Abbe refractometer. The experimental H_m^E data were correlated using the Redlich–Kister equation [18] and modeled with local composition models such as UNIQUAC [19], modified UNIFAC (Dortmund) [20] and NRTL [21] model to evaluate their predictive capabilities and gain insight into the molecular interactions present in these non-ideal systems. Meanwhile, the experimental data for density (ρ), speed of sound (u), refractive index (n_D), and isothermal compressibility (k_s) were correlated using a polynomial equation. Additionally, the density data were modeled using the Peng–Robinson equation of state (EoS) [8] and the PC-SAFT EoS [22].

2 Materials

All chemicals used in this work, including 22MEE ($C_5H_{12}O_3$), 22EEE ($C_6H_{14}O_3$), 2ME ($C_3H_8O_2$), 2-PhE ($C_8H_{10}O_2$), 2BE ($C_6H_{14}O_2$), and 2-PrOH (C_3H_8O) were purchased from Sigma-Aldrich. Each compound was supplied with a certified mass fraction purity exceeding 0.99, as specified by the manufacturer. Before conducting any measurements, the liquids were degassed in an ultrasonic bath (Fisher Scientific) to eliminate dissolved gases and prevent bubble formation that could interfere with densiometric accuracy. No additional purification procedures were applied. The mixtures were prepared by mass using an OHAUS analytical balance with a precision of ± 0.0001 g. A summary of the main physicochemical properties of the compounds is provided in Table 1.

3 Apparatus and Procedure

3.1 Excess Molar Enthalpies

Excess molar enthalpies (H_m^E) were measured at 0.1 MPa using a quasi-isothermal flow calorimeter (Fig. 1), previously validated in the literature [23]. The setup

Table 1 Purity and chemical data of studied liquids

Compound	Formula	Molar mass ($g \cdot mol^{-1}$)	Density ($g \cdot cm^{-3}$)		Stated purity[f] (mol %)	CAS number	Water content[g] (mass %)
			298.15 K	313.15 K			
22MEE*	$C_5H_{12}O_3$	120.15	1.0147[a]	1.0014[a]	> 99.0	111–77-3	≤ 0.03
22EEE*	$C_6H_{14}O_3$	134.18	0.9852[b]	0.9718[b]	> 99.0	111–90-0	≤ 0.03
2ME*	$C_3H_8O_2$	76.09	0.9598[c]	0.9460[c]	> 99.8	109–86-4	≤ 0.01
2-PhE*	$C_8H_{10}O_2$	138.18	1.1030[d]	1.0900[d]	> 99.0	122–99-6	≤ 0.02
2BE*	$C_6H_{14}O_2$	118.17	0.89705	0.8863	≥ 99.4	111–76-2	≤ 0.08
2-Propanol	C_3H_8O	60.10	0.7864[e]	0.7691[e]	≥ 99.5	67–63–0	≤ 0.02

[a]Lifi et al. [8]

[b]Lifi et al. [10]

[c]Lifi et al. [12]

[d]Makhlouf et al. [14]

[e]F. Zhou et al. [6]

[f]Purities were provided by the suppliers, and no purification was conducted for the studied compounds

[g]Water content was determined by Karl Fischer (KF) titration by the supplier Sigma-Aldrich

**22MEE* 2-(2-Methoxyethoxy)ethanol, *22EEE* 2-(2-Ethoxyethoxy)ethanol, *2ME* 2-Methoxyethanol, *2-PhE* 2-Phenoxyethanol, *2BE* 2-Buthoxyethanol

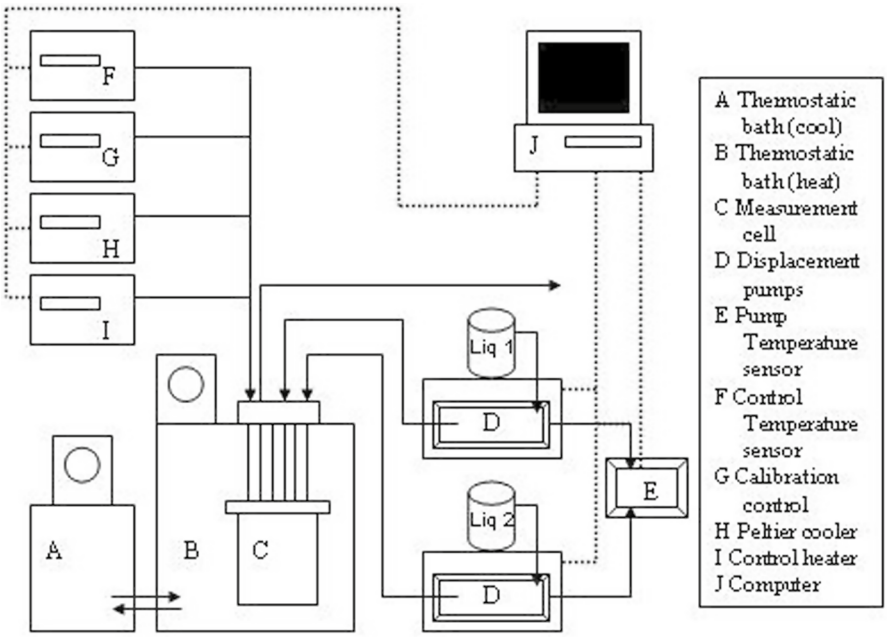

Fig. 1 Quasi-isothermal flow calorimeter. Schematic diagram

included two Agilent 1100 HPLC pumps delivering pure components through corrosion-resistant stainless-steel lines into a coiled mixer located within a temperature-controlled flow chamber. A thermostatic bath ensured temperature stability within ± 0.01 K. Mixture mole fractions (x_i) were determined from the molecular weights, flow rates, and densities of the pure substances, with densities interpolated from Table 1 data at the relevant temperatures. Various compositions were achieved by adjusting flow rates. The relative uncertainty of H_m^E was estimated at 1% (k = 2), and the standard uncertainty in x_i was ± 0.0005. An uncertainty budget for H_m^E, following EA-4/02 guidelines [24], is presented in Table 2.

3.2 Density, (ρ), Speed of Sound, (u), and Refractive Index, (n_D)

Density (ρ) and speed of sound (u) measurements at atmospheric pressure were obtained using an Anton Paar DSA 5000 M densitometer. This instrument uses a vibrating tube to determine density and an ultrasonic method to evaluate the speed of sound through the sample, allowing for precise and reliable data. The combined expanded uncertainty for ρ and u were estimated to be 0.003 g·cm^{-3} and 1.2 m·s^{-1}, respectively. The calibration of the apparatus was carried out with air and distilled water as reference fluids. Additionally, refractive index data (n_D) for all pure substances and their mixtures were measured using a digital Abbe refractometer (Abbemat 300, Anton Paar). This device works by analyzing the behavior of light as it passes through the sample. The refractometer was calibrated with air and water, and the expanded uncertainty in n_D was estimated to be ± 0.005 with a 95 % confidence level.

Table 2 Uncertainty budget for excess molar enthalpy using EA-4/02 [24]

		Units	Estimate	Divisor	Uncertainty value
$U(Q_{mixture})$	Resolution	W	$4{\cdot}10^{-6}$	$2\sqrt{3}$	0.8
$u(Q_{mixture})$	Repeatability		$4{\cdot}10^{-6}$	1	
$u(Q_{mixture})$	Non-linearity		$1.2{\cdot}10^{-4}$	1	
$U(\dot{V}_1)$	Accuracy	cm^3·s^{-1}	$2.5{\cdot}10^{-5}$	2	0.3
	Resolution		$2.5{\cdot}10^{-5}$	$2\sqrt{3}$	
$U(\dot{V}_2)$	Accuracy	cm^3·s^{-1}	$2.5{\cdot}10^{-5}$	2	0.3
	Resolution		$1.7{\cdot}10^{-5}$	$2\sqrt{3}$	
$u(T)$	Stability	K	$1{\cdot}10^{-2}$	1	0.1
$u(H_m^E)$	H_m^E = 400	J·mol^{-1}		k = 1	0.9
$U(H_m^E)$		J·mol^{-1}		k = 2	1.8
$U_r(H_m^E)$		J·mol^{-1}/J·mol^{-1}		k = 2	$5{\cdot}10^{-3}$

$Q_{mixture}$: heat of mixing; $\dot{V}_1$ and $\dot{V}_2$: flows of pure components 1 and 2 driven by isocratic pumps; T: temperature; H_m^E: excess molar enthalpy; x: mole fraction

Note that u represents the standard uncertainty, U is the expanded uncertainty with a stated coverage factor of k = 2, and U_r is the relative expanded uncertainty with a coverage factor stated in column "Divisor"

4 Modeling

This study applies various thermodynamic models to describe excess molar enthalpy and density in non-ideal mixtures. The NRTL and UNIQUAC models account for molecular interactions through local composition theory, while the modified UNIFAC (Dortmund) model predicts activity coefficients based on molecular group contributions, making it suitable when data are scarce. For the prediction of density, both the Peng–Robinson equation of state and the PC-SAFT equation were used, as they are well-suited for handling complex fluids and associating systems.

4.1 UNIQUAC Model

The UNIQUAC model describes the non-ideality of liquid mixtures by separating combinatorial and residual contributions, with the residual part expressed as [19]:

$$H_m^E = \sum\nolimits_{i=1}^{n} q_i x_i \frac{\sum_{j=1}^{n} \vartheta_j \Delta u_{ji} \tau_{ji}}{\sum_{j=1}^{n} \vartheta_j \tau_{ij}} \tag{1}$$

where $\vartheta_i = \frac{q_i x_i}{\sum_j q_j x_i}$ and q_i the surface area of a molecule is calculated by summing the contributions from its constituent functional groups.

4.2 Modified UNIFAC Model

The modified UNIFAC (Dortmund) model, a group-contribution extension of UNIQUAC, predicts activity coefficients by summing contributions from functional groups [20, 25].

$$H_m^E = -RT^2 \sum_i \sum_k x_i \upsilon_K^{(i)} \left[\left(\frac{\partial ln \Gamma_K}{\partial T} \right)_{p,x} - \left(\frac{\partial ln \Gamma_K^{(i)}}{\partial T} \right)_{p,x} \right] \tag{2}$$

$\upsilon_K^{(i)}$ is the number of groups of type k in molecule i. R and T stand for the universal gas constant and temperature, respectively.

4.3 NRTL Model

The NRTL model [21] accounts for local composition effects and uses an expression of the form:

$$H_m^E = -RT \sum\nolimits_{i=1}^{n} x_i \eta_i \tag{3}$$

Here, the mole fraction of component i is denoted by x_i, and η_i is computed as follows:

$$\eta_i = \frac{\sum_{k=1}^{p} x_k \tau_{ki} G_{ki} \left[\alpha \left(\tau_{ki} - \left(\sum_{n=1}^{p} x_n \tau_{ni} G_{ni} \Big/ \sum_{l=1}^{n} x_l G_{li} \right) \right) - 1 \right]}{\sum_{l=1}^{p} x_l G_{li}} \tag{4}$$

The non-randomness parameter α reflects variations in molecular interactions, leading to improved accuracy in phase behavior predictions. Gji is defined as:

$$G_{ji} = \exp\left(-\alpha \tau_{ij}\right) \tag{5}$$

where

$$\tau_{ij} = \left(g_{ij} - g_{ii}\right)/RT \tag{6}$$

Here, g_{ij} is the interaction energy between molecules i and j. The NRTL model is especially effective in systems with strong hydrogen bonding. In this research, the three-parameter version of the NRTL model with a variable α was employed.

4.4 PC-SAFT Model

The Perturbed Chain Statistical Associating Fluid Theory (PC-SAFT) equation of state, developed by Gross and Sadowski [22, 26], expresses the residual Helmholtz free energy ($\breve{a}^{res}$) as the sum of three contributions:

$$\breve{a}^{res} = \breve{a}^{hc} + \breve{a}^{disp} + \breve{a}^{assoc} \tag{7}$$

Here, $\breve{a}^{hc}$ corresponds to the hard-chain contribution, $\breve{a}^{disp}$ accounts for dispersive interactions, and $\breve{a}^{assoc}$ represents the association energy due to hydrogen bonding or other specific interactions.

The PC-SAFT model includes three primary parameters for non-associating fluids: the segment diameter (σ), the number of segments per molecule (m), and the segment energy parameter (ε/k). For associating components, two additional parameters are required: the association energy ($\varepsilon^{A_iB_i}$) and the association volume (k^{A_iBi}).

In mixtures, the interaction parameters σ_{ij} and ε_{ij} between dissimilar segments are evaluated using the Lorentz-Berthelot combining rules:

$$\sigma_{ij} = \left(\frac{\sigma_{ii} + \sigma_{jj}}{2}\right) \tag{8}$$

$$\varepsilon_{ij} = \sqrt{\varepsilon_{ii}\varepsilon_{jj}}\left(1 - k_{ij}\right) \tag{9}$$

Here, k_{ij} is the binary interaction parameter, used to correct for deviations in cross-interactions between unlike segments. In this study, k_{ij} is assumed to be zero for all mixtures.

The 2B association scheme, which considers two associating sites per molecule, was selected due to its effectiveness in representing the density of the studied liquid mixtures. The PC-SAFT model accounts explicitly for molecular size, shape, and association interactions, which is essential for accurate modeling of thermophysical properties in complex mixtures. Its formulation, grounded in statistical thermodynamics [27–29], provides a robust theoretical framework for describing fluid-phase behavior.

The PC-SAFT parameters were optimized by minimizing an objective function defined as:

$$Obj.F = \sum_{i=1}^{M} \left(\frac{\rho_i^{exp} - \rho_i^{calc}}{\rho_i^{exp}} \right)^2 \tag{10}$$

where M denotes the number of experimental data points, and ρ_i^{exp} and ρ_i^{calc} are the experimental and calculated densities, respectively.

4.5 Peng–Robinson model

To model fluid density, the Peng–Robinson equation relates pressure to temperature and molar volume, accounting for non-ideal molecular behavior [26, 8].

$$p = \frac{RT}{v - b} - \frac{a(T)}{v^2 + 2vb - b^2} \tag{11}$$

Here, R denotes the universal gas constant, while the parameters a and b are specific to each substance, representing molecular attraction and volume exclusion effects, respectively. Their values are determined from the fluid's critical properties.

$$b = \frac{0.007780 R T_c}{P_c} \tag{12}$$

$$a = a(T_c)\left[1 + k\left(1 - T_c^{0.5}\right)\right]^2 \tag{13}$$

$$a\left(T_c\right) = \frac{0.45724 R^2 T_c^2}{P_c} \tag{14}$$

$$k = 0.37464 + 1.54226\omega - 0.26992\omega^2 \tag{15}$$

where P_c and T_c represent the critical pressure and temperature of the fluid, respectively, and the coefficient k is calculated as a function of the acentric factor ω.

$$\omega = -\log\left(\frac{P}{P_c}\right)_{\frac{T}{T_c}=0.7} - 1 \tag{16}$$

The critical properties P_c, T_c, and the acentric factor ω for the pure compounds were obtained a data base [30].

When applying the Peng–Robinson equation of state to mixtures, the parameters a_{mix} and b_{mix} are calculated using the van der Waals mixing rules [31].

$$a_{mix} = \sum_i \sum_j x_i x_j a_{ij} \tag{17}$$

$$b_{mix} = \sum_i x_i b_i \tag{18}$$

$$a_{ij} = \left(a_{ii} a_{jj}\right)^2 \left(1 - K_{ij}\right) \tag{19}$$

Here, K_{ij} represents the binary interaction parameter between components i and j, which is often assumed to be zero when no specific interaction data is available. The term x_i denotes the mole fraction of component i in the mixture.

5 Correlation and Adjustment

5.1 Redlich–Kister (R–K) Correlation

The R–K equation [18] was employed in this study, as presented below:

$$R(x) = x_1.\left(1 - x_1\right).\sum_{i=1}^{N} A_i.(2x_1 - 1)^{i-1} \tag{20}$$

Here, $R(x)$ stands for a generic Redlich–Kister representation, applied to either H_m^E, Δn_D or V^E. In this context, x denotes the molar fraction, while n corresponds to the number of fitting parameters employed. The A_i coefficients are influenced by both the quality of the experimental data and the slope of the resulting curve [32]. To determine the optimal number of coefficients, Fisher's F-test [33] was applied.

5.2 Polynomial Adjustment

The properties ρ, and n_D for each binary mixture were correlated using a general polynomial expression of the form:

$$A(x) = \sum_{i=1}^{N} A_i.x_1^{i-1} \tag{21}$$

In this equation, A represents the physical property of interest (ρ, k_s, u or n_D); x_1 is the mole fraction of component 1; and A_i are the polynomial coefficients determined via an unweighted least-squares fitting procedure.

5.3 Statistical Parameters

To evaluate the accuracy and reliability of the correlated experimental data, several statistical indicators were computed:

- The Absolute Average Deviation (AAD) is defined as:

$$AAD(P) = \frac{100}{N}\sum_{i=1}^{N}\left|\frac{P^E_{m,exp} - P^E_{m,calc}}{P^E_{exp}}\right| \tag{22}$$

  Here, P^E_{exp} and P^E_{calc} represent the experimental and calculated values, respectively. Where P could be density, ρ, excess mola enthalpy, H^E_m, refractive index, n_D, or speed of sound, u.
- The standard deviation (σ) for each fitted property was calculated to assess the quality of the fit, using the formula:

$$\sigma(X) = \left[\sum_{i=1}^{N}\frac{(X_{exp} - X_{calc})^2}{(N-p)}\right]^{1/2} \tag{23}$$

  where, N is the total number of experimental points; p: the number of parameters used in the model; X_{exp}, X_{calc} are respectively the experimental and calculated value.

6 Results and Discussion

6.1 Excess Molar Enthalpy (H^E_m)

The thermodynamic behavior of binary mixtures containing glycol ethers with 2-PrOH are significantly influenced by molecular structure, intermolecular forces particularly hydrogen bonding and temperature effects. Experimental data for the H^E_m of five mixtures measured at $T = 298.15$ and 313.15 K under atmospheric pressure, are shown in Fig. 2 and listed in Tables 3 and 4. The adjustable parameters A_i derived from fitting Eq. 20 to the experimental H^E_m data for each binary mixture are presented in Table S1. The parameters used in the UNIQUAC and NRTL models to calculate H^E_m are listed in Table S2. As for the Modified UNIFAC (Dortmund) model, Tables 5, 6, and 7, and Table S3 provide the group surface volume values [34], necessary group interaction parameters, structural group assignments, and AAD deviation, respectively. In all cases, the curves display positive values of H^E_m, indicating that the mixing process is endothermic. This is mainly attributed to the

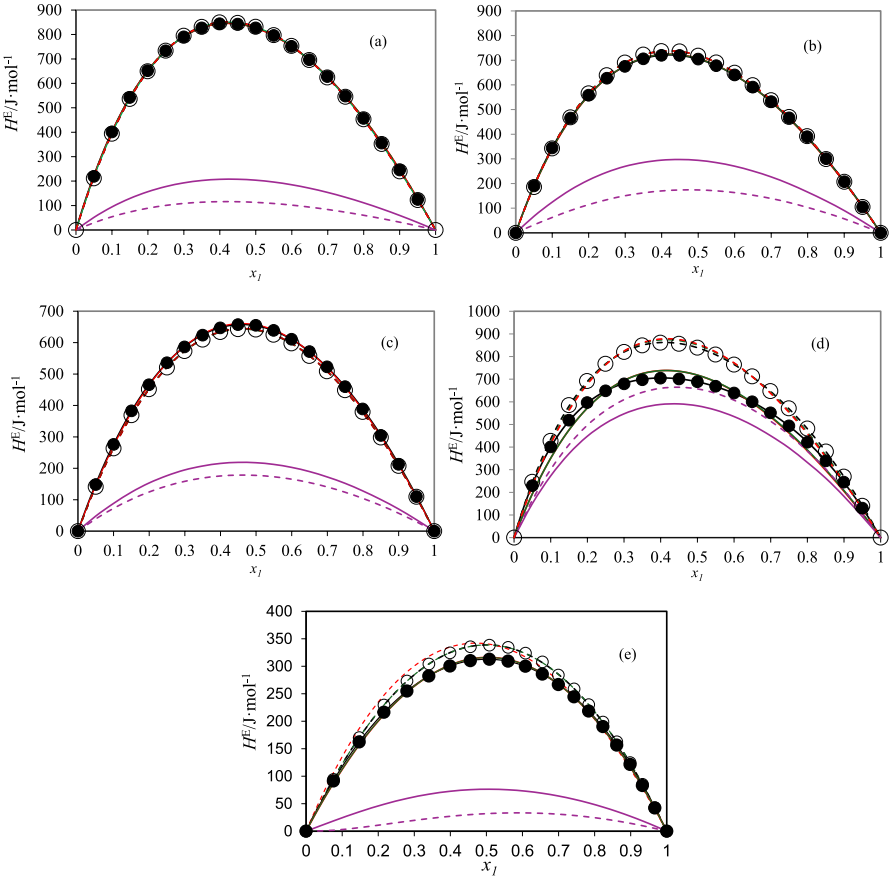

Fig. 2 Excess molar enthalpies,H_m^E, of (a) 2-(2-methoxyethoxy)ethanol + 2-propanol; (b) 2-(2-ethoxyethoxy)ethanol + 2-propanol; (c) 2-methoxyethanol + 2-propanol; (d) 2-phenoxyethanol + 2-propanol and (e) 2-buthoxyethanol + 2-propanol binary mixtures. At T = 298.15 K: ●, experimental data; (——), calculated values with Redlich–Kister (Eq. 20), (——), calculated values with NRTL model (Eq. 3); (——), calculated values with UNIQUAC model (Eq. 1), (——), calculated values with Modified UNIFAC (Dortmund) model (Eq. 2). At T = 313.15 K: ○, experimental data (—), calculated values with Redlich–Kister (Eq. 20), (—), calculated values with NRTL model (Eq. 3); (—), calculated values with UNIQUAC model (Eq. 1), (—), calculated values with Modified UNIFAC (Dortmund) model (Eq. 2)

disruption of strong hydrogen bonds present in pure substances and the formation of comparatively weaker interactions between the dissimilar components.

6.1.1 22MEE + 2-PrOH

As presented in Fig. 2a, the H_m^E for the 22MEE and 2-PrOH mixture remains positive across all compositions at both temperatures studied: 298.15 K and 313.15 K. This indicates an endothermic mixing process, where the energetic cost of disrupting strong self-associative hydrogen bonds in the pure components outweighs the

Table 3 Experimental data of excess molar enthalpy, H_m^E, of studied mixtures x_1 2-(2-methoxyethoxy) ethanol (1) + (1 − x_1) 2-propanol (2), x_1 2-(2-ethoxyethoxy)ethanol (1) + (1 − x_1) 2-propanol (2), x_1 2-methoxyethanol (1) + (1−x_1) 2-propanol (2), x_1 2-phenoxyethanol (1) + (1 − x_1) 2-propanol (2) and x_1 2-butoxyethanol (1) + (1 − x_1) 2-propanol (2) at T = 298.15 K and p = 0.1 MPa

x	H_m^E/J·mol^{-1}	x	H_m^E/J·mol^{-1}	x	H_m^E/J·mol^{-1}	x	H_m^E/J·mol^{-1}
x_1 2-(2-methoxyethoxy)ethanol (1) + (1 − x_1) 2-propanol (2)*							
0.0495	219.6	0.2996	790.6	0.5497	796.3	0.7994	456.8
0.0997	401.5	0.3495	827.4	0.5991	752.1	0.8498	355.9
0.1494	542.3	0.3991	844.3	0.6488	696.9	0.9001	245.8
0.1993	652.3	0.4495	843.0	0.6988	628.0	0.9502	125.2
0.2494	733.8	0.4993	827.6	0.7490	548.2		
x_1 2-(2-ethoxyethoxy)ethanol (1) + (1 − x_1) 2-propanol (2)*							
0.0501	190.4	0.2990	675.1	0.5492	678.3	0.7983	390.2
0.0995	344.4	0.3494	705.9	0.5996	640.5	0.8503	300.9
0.1498	465.8	0.3990	720.3	0.6493	591.2	0.9003	207.8
0.1995	558.4	0.4486	719.7	0.6997	532.3	0.9503	105.1
0.2494	627.0	0.4998	704.9	0.7488	466.6		
x_1 2-methoxyethanol (1) + (1 − x_1) 2-propanol (2)*							
0.0499	148.5	0.2989	586.4	0.5491	638.9	0.7989	389.1
0.0999	276.1	0.3497	623.7	0.5993	611.0	0.8500	304.7
0.1501	382.9	0.3993	646.9	0.6497	571.6	0.8999	212.7
0.1991	466.0	0.4490	657.3	0.6988	523.0	0.9499	110.1
0.2496	535.9	0.4990	655.1	0.7494	460.0		
x_1 2-phenoxyethanol (1) + (1 − x_1) 2-propanol (2)*							
0.0497	229.8	0.2999	679.6	0.5496	668.8	0.7999	421.6
0.0996	400.9	0.3495	697.3	0.5999	638.9	0.8506	339.6
0.1495	518.8	0.3990	704.5	0.6493	600.4	0.8992	245.2
0.1991	596.9	0.4496	701.2	0.6992	551.3	0.9497	130.3
0.2493	648.5	0.4999	688.7	0.7494	493.8		
x_1 2-butoxyethanol (1) + (1 − x_1) 2-propanol (2)*							
0.0757	91.3	0.3990	300.4	0.6552	285.7	0.8614	156.6
0.1472	162.4	0.4554	310.3	0.6995	266.7	0.8984	121.5
0.2157	216.3	0.5082	312.8	0.7429	244.4	0.9326	83.0
0.2797	255.0	0.5601	309.3	0.7836	218.5	0.9670	42.3
0.3404	282.4	0.6081	300.1	0.8231	190.2		

[a]Standard uncertainties of pressure p, temperature T and mole fraction x are as follows: $u(p)$ = 0.001 MPa, $u(T)$ = 0.05 K, $u(x)$ = 0.0005. The relative expanded uncertainty (k = 2) is $U_r(H_m^E)$ = 0.01 for excess molar enthalpy

*x_1: mole fraction of component (1) 2-(2-Methoxyethoxy)ethanol, 2-(2-Ethoxyethoxy)ethanol, 2-Methoxyethanol, 2-Phenoxyethanol or 2-Butoxyethanol

strength of new interactions formed in the mixture. The maximum H_m^E occurs near an equimolar composition at x_1 = 0.3991 with a value of 844.3 J·mol^{-1} at 298.15 K and at x_1 = 0.399 with 849.6 J·mol^{-1} at 313.15 K. The observed temperature dependence suggests that the non-ideality of the mixture becomes more pronounced at higher

Table 4 Experimental data of excess molar enthalpy, H_m^E, of studied mixtures x_1 2-(2-methoxyethoxy) ethanol (1) + (1 − x_1) 2-propanol (2), x_1 2-(2-ethoxyethoxy)ethanol (1) + (1 − x_1) 2-propanol (2), x_1 2-methoxyethanol (1) + (1 − x_1) 2-propanol (2), x_1 2-phenoxyethanol (1) + (1 − x_1) 2-propanol (2) x_1 2-butoxyethanol (1) + (1 − x_1) 2-propanol (2) at T = 313.15 K and p = 0.1 MPa

x	H_m^E/J·mol^{-1}	x	H_m^E/J·mol^{-1}	x	H_m^E /J·mol^{-1}	x	H_m^E/J·mol^{-1}
x_1 2-(2-methoxyethoxy)ethanol (1) + (1 − x_1) 2-propanol (2)*							
0.0495	211.5	0.2995	795.0	0.5497	797.6	0.7994	453.4
0.0997	394.1	0.3495	831.6	0.5990	753.6	0.8498	352.1
0.1494	536.5	0.3990	849.6	0.6486	695.9	0.9001	240.3
0.1993	649.7	0.4495	847.8	0.6988	624.4	0.9502	122.7
0.2494	734.0	0.4992	831.9	0.7490	545.4		
x_1 2-(2-ethoxyethoxy)ethanol (1) + (1 − x_1) 2-propanol (2)*							
0.0501	185.6	0.2990	690.5	0.5492	691.1	0.7983	392.0
0.0995	342.5	0.3494	722.8	0.5996	649.4	0.8503	299.3
0.1498	468.3	0.3990	736.9	0.6493	599.1	0.9003	207.1
0.1995	565.7	0.4486	735.9	0.6997	538.2	0.9503	105.0
0.2494	639.4	0.4998	718.5	0.7488	470.3		
x_1 2-methoxyethanol (1) + (1 − x_1) 2-propanol (2)*							
0.0499	141.1	0.2988	573.2	0.5489	624.9	0.7990	379.3
0.0999	263.4	0.3497	609.6	0.5992	597.6	0.8500	297.9
0.1501	369.1	0.3992	633.6	0.6495	557.4	0.8999	207.5
0.1990	451.8	0.4491	642.9	0.6987	508.7	0.9499	109.5
0.2496	520.9	0.4989	641.7	0.7494	448.5		
x_1 2-phenoxyethanol (1) + (1 − x_1) 2-propanol (2)*							
0.0496	246.7	0.2998	820.1	0.5493	808.7	0.7998	482.0
0.0995	427.5	0.3493	849.2	0.5997	764.6	0.8505	380.1
0.1494	585.3	0.3988	861.4	0.6491	712.4	0.8991	269.6
0.1991	691.8	0.4495	856.5	0.6990	647.5	0.9497	140.7
0.2492	768.0	0.4998	839.1	0.7493	571.1		
x_1 2-butoxyethanol (1) + (1 − x_1) 2-propanol (2)*							
0.0757	94.2	0.3990	324.6	0.6552	308.1	0.8614	162.8
0.1472	170.4	0.4554	335.6	0.6995	284.1	0.8984	124.9
0.2157	229.6	0.5082	338.5	0.7429	258.9	0.9326	85.3
0.2797	273.3	0.5601	334.5	0.7836	230.3	0.9670	42.9
0.3404	304.2	0.6081	323.9	0.8231	198.7		

[a]Standard uncertainties of pressure p, temperature T and mole fraction x are as follows: $u(p)$ = 0.001 MPa, $u(T)$ = 0.05 K, $u(x)$ = 0.0005. The relative expanded uncertainty (k = 2) is $U_r(H_m^E)$ = 0.01 for excess molar enthalpy

*x_1: mole fraction of component (1) 2-(2-Methoxyethoxy)ethanol, 2-(2-Ethoxyethoxy)ethanol, 2-Methoxyethanol, 2-Phenoxyethanol or 2-butoxyethanol

temperatures due to increased thermal motion weakening hydrogen-bonded structures. Both 2-PrOH and 22MEE can participate in hydrogen bonding through their hydroxyl groups. However, 22MEE also contains an ether linkage, which imparts a dual character to the molecule hydrophilic due to the ether and hydroxyl groups,

and moderately hydrophobic due to its extended aliphatic chain [36]. While the ether oxygen can engage in dipolar interactions and contribute to dispersion forces, it does not form strong hydrogen bonds compared to the hydroxyl group [37]. In the mixture, hydrogen bonds can form between unlike molecules (hetero-association), but these are generally weaker than the self-associative (homo-associative) hydrogen bonds that dominate in the pure components [38]. This reduction in interaction strength upon mixing is further influenced by the flexibility and spatial hindrance introduced by the ethylene glycol backbone of 22MEE, which may limit close molecular packing. As a result, the system exhibits a positive deviation from ideal behavior, reflected in the excess molar enthalpy values. In terms of model performance, the R–K equation provides the best correlation with experimental data, closely reproducing the magnitude and shape of the H_m^E curve, yielding AAD of 0.16 % at 298.15 K and 0.28 % at 313.15 K. The NRTL model also performs well, capturing the smooth variation of H_m^E with composition. The UNIQUAC model delivers reasonable approximation but slightly underestimates the H_m^E values near the maximum. The Modified UNIFAC (Dortmund) model, while capable of capturing the overall trend, tends to underpredict the excess molar enthalpy at elevated temperatures. This outcome highlights the challenge of modeling systems where specific interactions like hydrogen bonding play a significant role, especially when using predictive group-contribution approaches that may not fully reflect localized or temperature-sensitive effects. The binary mixture examined in this work has not, to date, been experimentally characterized according to available literature.

6.1.2 22EEE + 2-PrOH

Figure 2b illustrates the behavior of the H_m^E for the binary system composed of 22EEE and 2-PrOH across the entire composition range at two temperatures: 298.15 K and 313.15 K. At both temperatures, H_m^E values remain positive, indicating that the mixing process is energetically unfavorable from an enthalpic standpoint. This suggests that the energetic cost of disrupting the structured hydrogen-bonding networks within the pure components, particularly those in 2-propanol, is not entirely compensated by the formation of new interactions between the two components in the mixture. The H_m^E reaches its maximum near an equimolar composition 720.3 J·mol^{-1} at $x_1 = 0.399$ and 736.9 J·mol^{-1} at $x_1 = 0.3989$ at lower (298.15 K) and higher (313.15 K) temperatures, respectively highlighting the proportions at which intermolecular disruption is greatest. On a molecular level, this can be attributed to the interplay between the hydroxyl group of 2-PrOH and the ether and hydroxyl groups of 22EEE. While hydrogen bonding is possible between these molecules, the presence of the ethyl group in 22EEE introduces steric hindrance and reduces the overall polarity compared to 22MEE. This structural variation weakens the strength and efficiency of hydrogen bond formation with 2-PrOH, resulting in a less energetically favorable interaction landscape [39]. Additionally, the longer side chain in 22EEE introduces more van der Waals interactions, which are generally weaker and less directional than hydrogen bonds, further contributing to the positive H_m^E values [40]. The increase in H_m^E with rising temperature implies that thermal agitation disrupts hydrogen-bonded structures more readily, decreasing the extent of favorable interactions in the mixture

and thereby amplifying deviations from ideal mixing behavior. This effect reflects the dynamic nature of hydrogen bonds, which become less stable as thermal energy increases. Regarding the modeling results, the R–K expansion best reproduces the shape and magnitude of the experimental H_m^E curves, confirming its suitability for correlating symmetric systems with regular enthalpy trends, yielding AAD of 0.24 % at 298.15 K and 0.35 % at 313.15 K. The NRTL model captures the excess molar enthalpy variation across compositions more accurately due to its treatment of local non-randomness, while UNIQUAC slightly underestimates the H_m^E peak, likely from its simplified size and surface area assumptions. The Modified UNIFAC (Dortmund) model, although useful for predicting general trends, consistently underestimates H_m^E, particularly at higher temperatures. This is likely due to its reliance on generic group interaction parameters, which may not accurately reflect the specific, temperature-sensitive hydrogen bonding interactions occurring in this system. No experimental data for the studied binary mixture were found in the literature.

6.1.3 2ME + 2-PrOH

Figure 2c illustrates the variation of H_m^E for mixtures of 2ME and 2-PrOH at two temperatures: 298.15 K and 313.15 K. The results indicate that H_m^E remains positive across the full molar ratio range at both temperatures, signifying that the mixing process is endothermic. This suggests that the energy required to break the strong self-associative hydrogen bonds in the pure components, especially in 2-PrOH, is greater than the energy released when new interactions form between the two components upon mixing. The most pronounced enthalpic deviations occur near the equimolar region, where the maximum values of H_m^E reach 657.3 J·mol^{-1} at $x_1 = 0.449$ and 642.9 J·mol^{-1} at $x_1 = 0.4491$ for 298.15 K and 313.15 K, respectively. These are the highest maxima observed among all the binary systems studied, indicating significant non-ideal behavior. This can be attributed to the molecular structure of 2ME, which contains both ether and hydroxyl groups, making it highly interactive but also capable of disrupting existing hydrogen-bonding networks. The small size and strong polarity of 2ME allow it to interact closely with 2-PrOH molecules, however, the new interactions that arise are likely weaker or less directional than those present in the pure substances, resulting in a net enthalpic decrease [41]. The increase in H_m^E with rising temperature reflects the destabilization of hydrogen bonds due to thermal motion. As temperature increases, the extent of molecular association decreases, amplifying the deviation from ideality and leading to higher H_m^E values.

Regarding model performance, the R–K polynomial provides an excellent representation of the experimental data, accurately describing both the shape and magnitude of the H_m^E curve, yielding AAD of 0.25 % at 298.15 K and 0.23 % at 313.15 K. The NRTL model also shows good agreement, especially around the maximum. Although the UNIQUAC model slightly underestimates the H_m^E peak, it still captures the overall trend of the data. The Modified UNIFAC (Dortmund) model, while useful for predicting general behavior, underestimates the H_m^E values, particularly at higher temperatures. This underperformance reflects the limitations of group contribution methods, which may not adequately describe temperature-sensitive, specific interactions such as hydrogen bonding in systems involving small, highly polar

Table 5 Modified UNIFAC (Dortmund) relative Van der Waals volumes R_K and surface areas Q_K [34, 35]

Main group	Subgroup	R_K	Q_K
CH_2	CH_3	0.9011	0.848
	CH_2	0.6744	0.540
	CH	0.6325	0.355
OH	OH	1.0000	1.200
CH_2O	CH_3O	1.1450	1.088
	CH_2O	0.9183	0.780
ACOH	ACOH	0.8952	0.680

Table 6 Modified UNIFAC (Dortmund) group interaction parameters used in this work

Main group		Group interaction parameters		
1	2	a_{12}/K	b_{12}/K	c_{12}/K^{-1}
		a_{21}/K	b_{21}/K	c_{21}/K^{-1}
CH_2	OH	2777	− 4.674	0.001551
		1606	− 4.746	0.0009181
CH_2	CH_2O	233.1	− 0.3155	–
		− 9.654	− 0.03242	–
CH_2	ACOH	1381	− 0.9977	–
		1987	− 4.615	–
OH	CH_2O	816.7	− 5.092	0.00606
		650.9	− 0.7132	0.000815
OH	ACOH	83.91	− 1.262	–
		465.4	− 1.841	–

molecules like 2ME. The studied binary system has not been experimentally investigated in existing literature.

6.1.4 2PhE + 2-PrOH

A closer look at Fig. 2d reveals that the H_m^E for 2PhE and 2-PrOH system remains positive throughout the entire mole fraction range at both 298.15 K and 313.15 K. This consistent endothermic behavior indicates that the mixing process involves a net absorption of energy, which is typically associated with the breakdown of strong self-associative hydrogen bonds in the pure components. The intermolecular interactions formed upon mixing are not sufficiently strong to offset this energetic disruption. The maximum excess molar enthalpy appears near equimolar compositions, with values of 704.5 J·mol^{-1} at $x_1 = 0.399$ and 861.4 J·mol^{-1} at $x_1 = 0.3988$ at both temperatures, respectively. These moderate values suggest that the interaction between 2PhE and 2-PrOH, while not negligible, is less intense than those observed in systems with smaller, more flexible glycol ethers. From a molecular perspective, the bulky phenyl ring in 2PhE introduces steric hindrance and reduces the molecule's ability to form efficient hydrogen bonds with 2-PrOH [42]. Although both

Table 7 Molecular formulae of the species in this work, shown as structures of subgroups for group-contribution models

Component	Structure	Molecular formula
2-(2-methoxyethoxy)ethanol	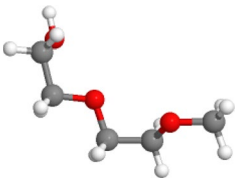	$CH_3O–CH_2–CH_2O–CH_2–CH_2–OH$
2-(2-ethoxyethoxy)ethanol	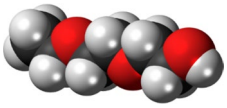	$CH_3–CH_2O–CH_2–CH2O–CH_2–CH_2–OH$
2-methoxyethanol	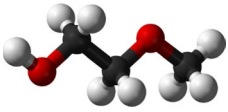	$CH_3O–CH_2–CH_2–OH$
2-phenoxyethanol	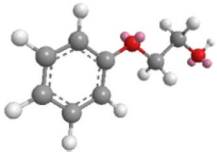	$C_6H_5O–CH_2–CH_2–OH$
2-butoxyethanol	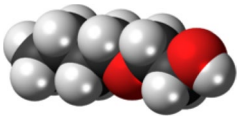	$CH_3–(CH_2)_2–CH_2O–CH_2–CH_2–OH$
2-Propanol	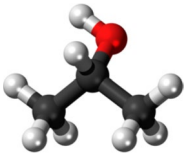	$CH3–CH–OH–CH_3$

components possess hydroxyl groups capable of hydrogen bonding, the spatial orientation and rigidity of the aromatic structure limit their effectiveness in forming strong, directional interactions. In addition, the presence of the aromatic ring may contribute to weak dispersion or π–π interactions, which are generally less energetically favorable compared to hydrogen bonding [43]. These interactions may slightly stabilize the mixture but are not strong enough to compensate for the loss of self-association in the pure liquids. The increase in H_m^E with temperature further supports the interpretation that thermal motion disrupts existing interactions, weakening hydrogen bonds and increasing the system's deviation from ideality.

Among the tested thermodynamic models, the R–K polynomial yields the closest fit to the experimental data, accurately representing both the shape and intensity of the H_m^E curve, yielding AAD of 0.32 % at 298.15 K and 0.37 % at 313.15 K. The NRTL model performs comparably well, providing a smooth and continuous

Table 8 (continued)

x_1	ρ/(g·cm^{-3})	u/(m·s^{-1})	Ks (10^{12} Pa^{-1})	n_D
0.1929	0.8227	1121.9	965.69	1.3801
0.3006	0.8534	1157.17	875.08	1.3867
0.4029	0.8798	1189.12	803.87	1.3909
0.5044	0.9036	1218.55	745.33	1.3961
0.606	0.9253	1244.71	697.59	1.4009
0.7002	0.9438	1268.02	658.96	1.4043
0.7965	0.9616	1291.61	623.38	1.4076
0.8945	0.9782	1315.17	567.50	1.4112
1.0000	0.9949	1334.64	564.30	1.4144
{22EEE (1) + 2-PrOH (2)}				
T = 293.15 K				
0.0000	0.7851	1156.33	952.59	1.3771
0.1023	0.8197	1195.72	853.29	1.3851
0.2006	0.8484	1227.55	782.17	1.3922
0.2985	0.8736	1255.42	726.32	1.3992
0.4047	0.8976	1282.88	676.95	1.4043
0.5012	0.9167	1305.68	639.88	1.4090
0.5994	0.9340	1326.34	608.63	1.4133
0.6903	0.9483	1344.01	583.77	1.4169
0.7905	0.9627	1361.57	560.29	1.4204
0.9016	0.9770	1379.65	537.72	1.4239
1.0000	0.9886	1394.02	520.52	1.4273
T = 303.15 K				
0.0000	0.7767	1121.65	1023.41	1.3728
0.1023	0.8112	1160.92	914.66	1.3811
0.2006	0.8398	1192.85	836.85	1.3880
0.2985	0.8649	1220.75	775.88	1.3949
0.4047	0.8886	1248.07	722.44	1.4006
0.5012	0.9077	1270.81	682.21	1.4050
0.5994	0.9249	1291.44	648.28	1.4092
0.6903	0.9393	1309.07	621.25	1.4128
0.7905	0.9537	1325.53	596.80	1.4163
0.9016	0.9682	1344.58	571.31	1.4199
1.0000	0.9797	1359.04	552.61	1.4229
T = 313.15 K				
0.0000	0.7644	1086.5	1108.28	1.3683
0.1023	0.8015	1125.86	984.30	1.3774
0.2006	0.8309	1157.9	897.68	1.3840
0.2985	0.8557	1185.88	830.99	1.3910
0.4047	0.8795	1213.53	772.12	1.3976
0.5012	0.8987	1235.53	728.89	1.4012
0.5994	0.9162	1257.64	690.08	1.4050
0.6903	0.9304	1274.38	661.82	1.4087

Table 8 (continued)

x_1	ρ/(g·cm^{-3})	u/(m·s^{-1})	Ks (10^{12} Pa^{-1})	n_D
0.7905	0.9446	1291.84	634.34	1.4122
0.9016	0.9592	1309.75	607.71	1.4157
1.0000	0.9708	1324.1	587.53	1.4186
T = 323.15 K				
0.0000	0.7587	1050.88	1193.47	1.3637
0.1023	0.7931	1090.55	1060.18	1.3740
0.2006	0.8219	1122.86	965.04	1.3821
0.2985	0.8466	1151.01	891.58	1.3879
0.4047	0.8704	1178.78	826.86	1.3942
0.5012	0.8896	1201.28	779.00	1.3975
0.5994	0.9070	1223.16	736.93	1.4011
0.6903	0.9215	1239.89	705.92	1.4048
0.7905	0.9359	1257.19	676.05	1.4081
0.9016	0.9503	1275.6	646.69	1.4116
1.0000	0.9618	1289.49	625.30	1.4143
{2ME (1) + 2-PrOH (2)}				
T = 298.15 K				
0.0000	0.7851	1156.33	952.59	1.3771
0.1019	0.8038	1179.09	894.86	1.3798
0.2034	0.8222	1196.01	850.22	1.3824
0.3018	0.8401	1215.27	805.98	1.3849
0.4020	0.8582	1234.79	764.24	1.3875
0.5008	0.8759	1254.73	725.14	1.3900
0.6012	0.8940	1275.36	687.70	1.3925
0.7012	0.9119	1296.85	652.01	1.3950
0.8000	0.9295	1316.97	620.32	1.3975
0.8962	0.9465	1337.38	590.72	1.3999
1.0000	0.9647	1360.37	560.16	1.4024
T = 303.15 K				
0.0000	0.7767	1121.65	1023.41	1.3728
0.1019	0.7952	1144.09	960.72	1.3755
0.2034	0.8136	1161.27	911.48	1.3782
0.3018	0.8313	1180.6	863.02	1.3807
0.4020	0.8493	1200.23	817.40	1.3833
0.5008	0.8670	1220.84	773.84	1.3859
0.6012	0.8850	1240.84	733.85	1.3884
0.7012	0.9029	1261.78	695.65	1.3909
0.8000	0.9204	1282.56	660.50	1.3933
0.8962	0.9373	1302.88	628.49	1.3958
1.0000	0.9556	1325.78	595.34	1.3983

Table 8 (continued)

x_1	ρ/(g·cm^{-3})	u/(m·s^{-1})	Ks (10^{12} Pa^{-1})	n_D
T = 313.15 K				
0.0000	0.7644	1086.5	1108.28	1.3683
0.1019	0.7850	1108.76	1036.28	1.3712
0.2034	0.8046	1126.26	979.80	1.3739
0.3018	0.8224	1145.32	927.01	1.3766
0.4020	0.8401	1166.87	874.25	1.3794
0.5008	0.8579	1184.99	830.09	1.3821
0.6012	0.8758	1205.83	785.24	1.3846
0.7012	0.8940	1227.14	742.80	1.3870
0.8000	0.9112	1247.87	704.78	1.3894
0.8962	0.9280	1268.09	670.09	1.3917
1.0000	0.9463	1291.09	633.95	1.3942
T = 323.15 K				
0.0000	0.7587	1050.88	1193.47	1.3637
0.1019	0.7771	1073.29	1117.06	1.3671
0.2034	0.7954	1091.02	1056.26	1.3700
0.3018	0.8130	1110.33	997.73	1.3728
0.4020	0.8308	1132.08	939.16	1.3755
0.5008	0.8485	1150.28	890.73	1.3780
0.6012	0.8665	1171.29	841.25	1.3805
0.7012	0.8842	1191.92	796.05	1.3830
0.8000	0.9017	1213.2	753.50	1.3853
0.8962	0.9186	1233.83	715.09	1.3876
1.0000	0.9367	1255.74	677.00	1.3901
{2PhE (1) + 2-PrOH (2)}				
T = 293.15 K				
0.0000	0.7851	1156.33	952.59	1.3771
0.1035	0.8395	1227.36	790.79	1.4042
0.2014	0.8839	1284.43	685.77	1.4271
0.2989	0.9225	1335.5	607.77	1.4461
0.4025	0.9596	1385.46	542.91	1.4645
0.5000	0.9922	1429.2	493.43	1.4800
0.5958	1.0178	1466.12	457.10	1.4936
0.6989	1.0439	1503	424.07	1.5069
0.7938	1.0658	1533.56	398.97	1.5179
0.8915	1.0856	1561.41	377.84	1.5282
1.0000	1.1072	1591.29	356.66	1.5387
T = 303.15 K				
0.0000	0.7767	1121.65	962.95	1.3728
0.1035	0.8306	1191.56	847.94	1.4005
0.2014	0.8751	1249.7	731.73	1.4224
0.2989	0.9148	1303.48	643.38	1.4418

Table 8 (continued)

x_1	ρ/(g·cm^{-3})	u/(m·s^{-1})	Ks (10^{12} Pa^{-1})	n_D
0.4025	0.9519	1351.52	575.15	1.4604
0.5000	0.9838	1394.65	522.60	1.4810
0.5958	1.0090	1431.5	483.66	1.4900
0.6989	1.0349	1467.62	448.60	1.5024
0.7938	1.0566	1498.42	421.52	1.5136
0.8915	1.0780	1526.74	397.98	1.5238
1.0000	1.0987	1556.67	375.59	1.5363
T = 313.15 K				
0.0000	0.7644	1086.5	1108.28	1.3683
0.1035	0.8185	1156.88	912.89	1.3960
0.2014	0.8651	1214.19	784.10	1.4239
0.2989	0.9058	1270.83	683.62	1.4391
0.4025	0.9429	1318.2	610.34	1.4564
0.5000	0.9740	1359.31	555.66	1.4758
0.5958	1.0013	1399.4	509.99	1.4851
0.6989	1.0278	1435.15	472.38	1.4998
0.7938	1.0492	1465.95	443.50	1.5093
0.8915	1.0700	1494.07	418.69	1.5199
1.0000	1.0901	1522.58	395.71	1.5298
T = 323.15 K				
0.0000	0.7587	1050.88	1193.47	1.3637
0.1035	0.8121	1121.9	978.30	1.3947
0.2014	0.8566	1180.43	837.81	1.4151
0.2989	0.8963	1233.06	733.78	1.4389
0.4025	0.9335	1283.67	650.07	1.4544
0.5000	0.9641	1325.25	590.58	1.4684
0.5958	0.9920	1363.32	542.38	1.4822
0.6989	1.0178	1399.88	501.39	1.4945
0.7938	1.0407	1432.37	468.35	1.5050
0.8915	1.0611	1460.36	441.92	1.5157
1.0000	1.0815	1488.64	417.25	1.5254
{2BE (1) + 2-PrOH (2)}				
T = 293.15 K				
0.0000	0.7851	1156.33	952.59	1.3771
0.1033	0.8053	1186.99	881.34	1.3855
0.2004	0.8216	1211.65	829.03	1.3903
0.3010	0.8370	1232.22	786.89	1.3956
0.4050	0.8499	1250.35	752.63	1.4006
0.5061	0.8613	1266.33	724.06	1.4049
0.6022	0.8709	1280.28	700.51	1.4082
0.7009	0.8798	1293.23	679.61	1.4116
0.7961	0.8877	1304.79	661.67	1.4144

Table 8 (continued)

x_1	ρ/(g·cm^{-3})	u/(m·s^{-1})	Ks (10^{12} Pa^{-1})	n_D
0.8928	0.8950	1315.54	645.64	1.4171
1.0000	0.9025	1325.7	630.49	1.4197
T = 303.15 K				
0.0000	0.7767	1121.65	1023.41	1.3728
0.1033	0.7968	1152.06	945.57	1.3819
0.2004	0.8130	1175.73	889.82	1.3863
0.3010	0.8284	1197.62	841.62	1.3916
0.4050	0.8420	1215.84	803.44	1.3965
0.5061	0.8537	1231.84	771.99	1.4006
0.6022	0.8633	1245.97	746.16	1.4040
0.7009	0.8721	1259.29	723.05	1.4073
0.7961	0.8800	1270.86	703.60	1.4103
0.8928	0.8876	1281.61	685.93	1.4130
1.0000	0.8950	1291.77	669.60	1.4155
T = 313.15 K				
0.0000	0.7644	1086.5	1108.28	1.3683
0.1033	0.7850	1116.79	1021.38	1.3775
0.2004	0.8034	1141.04	956.02	1.3827
0.3010	0.8190	1161.64	904.87	1.3878
0.4050	0.8327	1180.88	861.19	1.3938
0.5061	0.8444	1197.61	825.71	1.3965
0.6022	0.8540	1211.53	797.77	1.4003
0.7009	0.8633	1224.94	771.99	1.4031
0.7961	0.8715	1236.57	750.41	1.4064
0.8928	0.8790	1247.49	731.04	1.4087
1.0000	0.8863	1257.69	713.31	1.4113
T = 323.15 K				
0.0000	0.7587	1050.88	1193.47	1.3637
0.1033	0.7788	1081.12	1098.63	1.3749
0.2004	0.7950	1105.77	1028.70	1.3810
0.3010	0.8101	1127.04	971.87	1.3860
0.4050	0.8236	1146.21	924.23	1.3881
0.5061	0.8354	1162.98	885.01	1.3933
0.6022	0.8454	1177.67	852.90	1.3954
0.7009	0.8546	1190.58	825.48	1.3990
0.7961	0.8627	1202.64	801.41	1.4019
0.8928	0.8701	1213.59	780.34	1.4045
1.0000	0.8776	1223.92	760.64	1.4070

[a]Standard uncertainties of pressure p, temperature T, are as follows: $u(p)$ = 0.004 MPa, $u(T)$ = 0.02 K. The expanded uncertainty of mole fraction x is $U(x)$= 0.0008. The combined expanded uncertainties U_c in density ρ, speed of sound u, and refractive index n_D are as follow: $U_c(\rho)$ = 0.003 g·cm^{-3}, $U_c(u)$ = 1.2 m·s^{-1}, and $U_c(n_D)$ = 0.005, with a 0.95 level of confidence

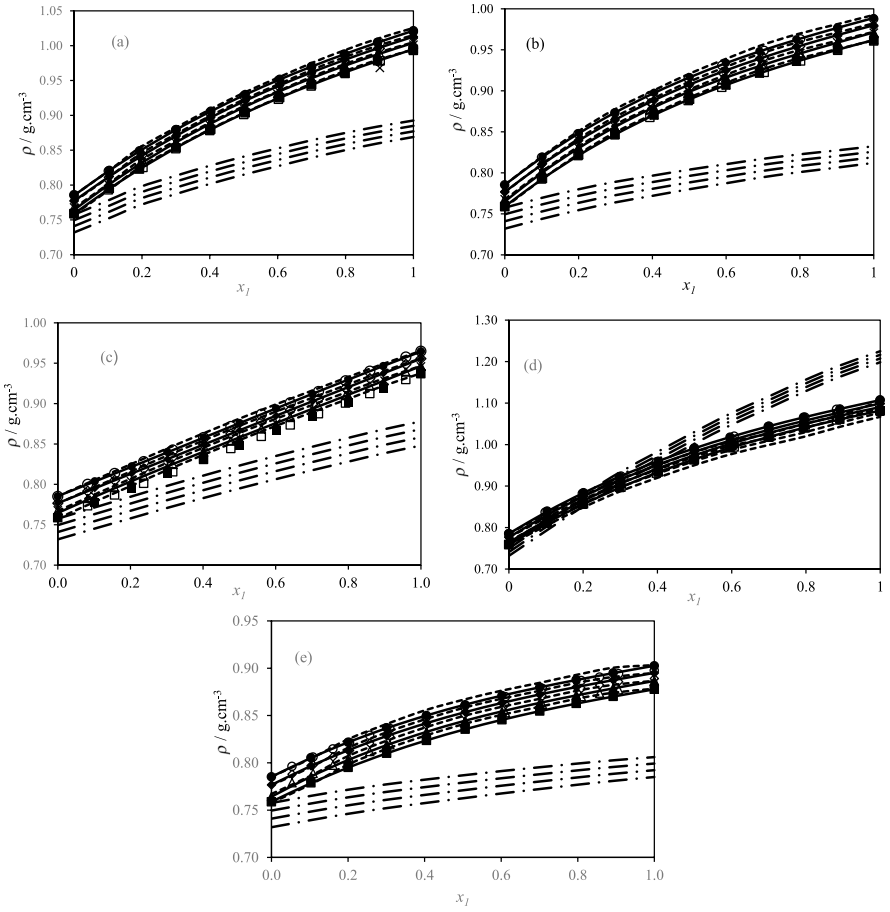

Fig. 3 Experimental values of densities, ρ, for the studied binary mixtures: (a) 2-(2-methoxyethoxy)ethanol (1) + 2-propanol (2): Experimental data in this work: (●), at 293.15 K, (◆), at 303.15 K, (▲), at 313.15 K, (■), at 323.15 K; (o), Belhadj et al. [45] at 293.15 K, (◇), Belhadj et al. [45] at 303.15 K, (Δ), Belhadj et al. [45] at 313.15 K, (+), Abala et al. [46] at 313.15 K, (□), Belhadj et al. [45] at 323.15 K. (b) 2-(2-ethoxyethoxy)ethanol (1) + 2-propanol (2): Experimental data in this work: (●), at 293.15 K, (◆), at 303.15 K, (▲), at 313.15 K, (■), at 323.15 K; o, Ouaar et al. [47] at 293.15 K, ◇, Ouaar et al. [47] at 303.15 K, Δ, Ouaar et al. [47] at 313.15 K, +, Abala et al. [46] at 313.15 K, □, Ouaar et al. [47] at 323.15 K. (c) 2-methoxyethanol (1) + 2-propanol (2): Experimental data in this work: (●), at 293.15 K, (◆), at 303.15 K, (▲), at 313.15 K, (■), at 323.15 K; o, Zarei et al. [48] at 293.15 K, ◇, Zarei et al. [48] at 303.15 K, Δ, Zarei et al. [48] at 313.15 K, +, Abala et al. [46] at 313.15 K, □, Zarei et al. [48] at 323.15 K. (d) 2-phenoxyethanol (1) + 2-propanol (2): Experimental data in this work: (●), at 293.15 K, (◆), at 303.15 K, (▲), at 313.15 K, (■), at 323.15 K; o, Makhlouf et al. [14] at 293.15 K, ◇, Makhlouf et al. [14] at 303.15 K, Δ, Makhlouf et al. [14] at 313.15 K, Δ, Makhlouf et al. [14] at 313.15 K, □, Makhlouf et al. [14] at 323.15 K. (e) 2-buthoxyethanol (1) + 2-propanol: Experimental data in this work: (●), at 293.15 K, (◆), at 303.15 K, (▲), at 313.15 K, (■), at 323.15 K; o, Dubey et al. [49] at 293.15 K, ◇, Dubey et al. [49] at 303.15 K, Δ, Dubey et al. [49] at 313.15 K, (solid line) polynomial equation, (dotted line) PC-SAFT equation (Eq. 7), (dashed line) Peng–Robinson equation (Eq. 11)

Table 9 PC-SAFT parameters for the pure compounds considered in this work

Compound	m[-]	σ [A]	ε/K [K]	ϵ^{AB}/K [K]	K^{AB}	AAD %
22MEE	5.3913	3.10393	227.797	1920.95	0.0327234	$1.65\,10^{-4}$
22EEE	5.74342	3.18681	230.644	1544.38	0.0358667	$2.00\,10^{-4}$
2ME	4.98311	2.82126	266.361	1792.03	0.0135779	$4.54\,10^{-6}$
2-PhE	3.8767	3.52531	200.01	3000	0.0752282	$7.00\,10^{-2}$
2BE	3.93576	3.55106	210.06	2927.62	0.069592	$1.33\,10^{-5}$
2-PrOH	5.43534	2.65575	205.083	1501.5	0.0627704	$3.00\,10^{-4}$

Table 10 Pure component data for the Peng–Robinson EoS [30]

Compound	T_c [K]	P_c [bar]	ω
22MEE	630	35.45	0.635
22EEE	656	30.53	0.7
2ME	564	50.84	0.387
2-PhE	698.15	36	0.806
2BE	633.9	32.7	0.521
2-PrOH	508.31	47.64	0.669

studied binary using Eq. 21 are listed in Table S4. Table 9 provides the PC-SAFT EoS parameters corresponding to the components investigated, while Table 10 lists the Peng–Robinson EoS parameters used for the studied components [30].

6.2.1 Density (ρ)

All the binary systems investigated, density decreases systematically as temperature increases, which aligns with the typical thermal expansion observed in liquids. The composition-dependent density profiles for each mixture exhibit smooth and continuous changes, indicating complete miscibility and gradual structural adjustments within the liquid phase as the proportions of components vary.

Among the binary mixtures analyzed, the polynomial model gives the most accurate representation of the experimental densities due to its empirical nature. However, the PC-SAFT model also performs well demonstrating its ability to reflect the main physical behaviors of the systems. This level of agreement suggests that PC-SAFT appropriately accounts for molecular features such as association, shape, and size, which play a key role in modeling complex liquid mixtures. Although some deviations are observed especially at lower temperatures or in mixtures involving bulky or highly polar compounds PC-SAFT remains significantly more reliable than the Peng–Robinson equation. The latter tends to underestimate density values, particularly for systems with strong intermolecular interactions, due to its limited treatment of associating effects. Overall, PC-SAFT offers a solid compromise between predictive power and physical relevance, especially when experimental data are limited or when dealing with structurally diverse mixtures.

6.2.2 Speed of Sound *(u)*

For all studied systems, the speed of sound changes non-linearly with mole fraction as shown in Fig. 4, indicating that the interactions between the components are not ideal. Typically, mixtures exhibit a maximum or minimum in sound velocity at intermediate compositions, suggesting the presence of structural or energetic effects such as hydrogen bonding and molecular association.

As temperature increases, the speed of sound generally decreases, reflecting the weakening of intermolecular forces due to thermal expansion and reduced density. This behavior is consistent across all systems and aligns with expectations for associating liquid mixtures.

The solid lines represent values obtained using a polynomial fit. The close agreement between experimental and calculated values indicates that the applied correlation provides a reliable representation of the system's acoustic behavior over the range of compositions and temperatures studied.

6.2.3 Refractive Index *(n_D)*

Figure 5 displays how the refractive index (n_D) evolves with mole fraction x_1 for the five binary systems. Across all systems, the refractive index shows a non-linear dependence on composition, which points to non-ideal mixing behavior and intermolecular interactions between the components. As the temperature increases, a general decrease in refractive index is observed consistent with the expected thermal effect on liquid density and molecular interactions. Mixtures richer in glycol ethers generally exhibit higher refractive indices, reflecting their stronger polarizability compared to 2-PrOH. Notably, the mixture involving 2-PhE reaches the highest values, likely due to its aromatic character, which enhances its optical response. The polynomial equation closely follows the experimental trends. The good agreement between calculated and measured data confirms the effectiveness of the chosen correlation in capturing the composition and temperature dependence of n_D.

6.2.4 Comparison with Literature Data

6.2.4.1 For Pure Component The thermophysical properties of the pure components investigated in this study were compared with reliable literature data [12, 14, 45–50], showing very good consistency overall. For density data, 2-PrOH showed excellent agreement, with the smallest AAD of 0.001 % reported at 293.15 K (with Makhlouf et al. [14] and Zarei et al. [48]) and the highest of 0.4 % showed at 313.15 K (with Abala et al. [46]). Similar levels of agreement were observed for the other pure components. The lowest density AADs were 0.02 % for both 2ME (with Zarei et al. [48]) and 2PhE (with Makhlouf et al. [14]) at 293.15 K, while the highest was 0.30 % at 303.15 K for 2BE (with Dubey et al. [49]). At 293.15 K, an AAD of 0.15 % was reported for 22MEE (with Belhadj et al. [45]), while 22EEE showed an AAD of 0.13 % (with Ouaar et al. [47]).

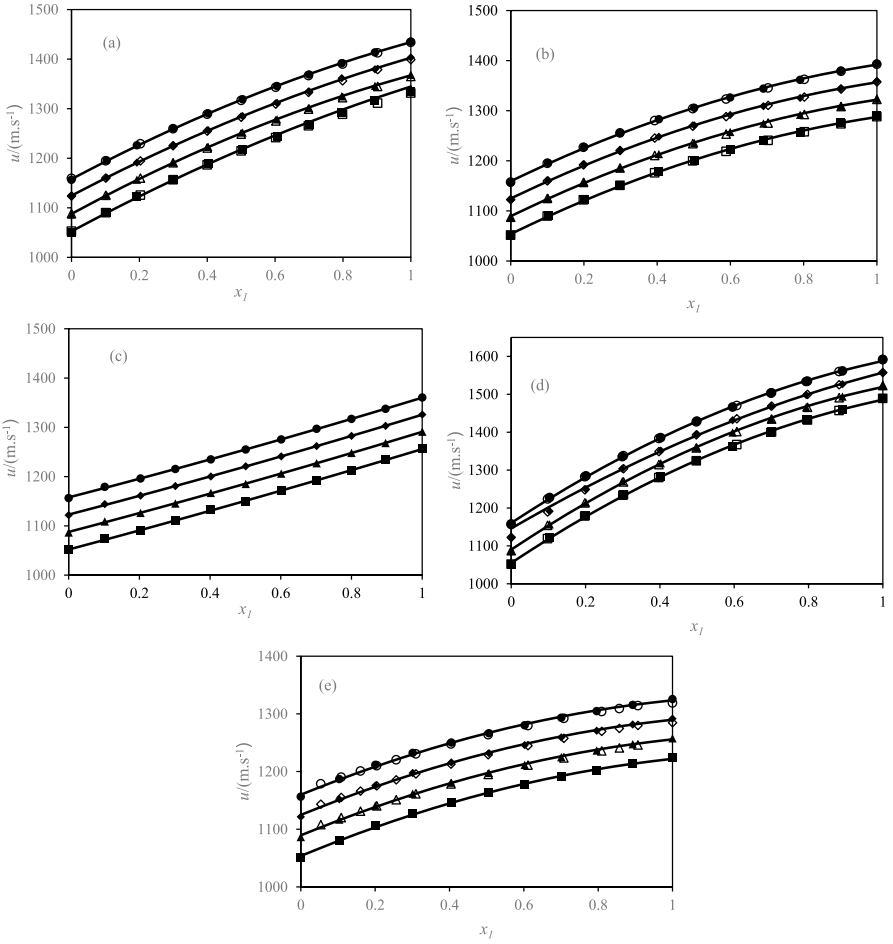

Fig. 4 Experimental values of speed of sound, u, as a function of mole fraction of x_1 for binary mixtures mixture (a) 2-(2-methoxyethoxy)ethanol (1) + 2-propanol (2): Experimental data in this work: (●), at 293.15 K, (◆), at 303.15 K, (▲), at 313.15 K, (■), at 323.15 K; o, Belhadj et al. [45] at 293.15 K, ◇, Belhadj et al. [45] at 303.15 K, Δ, Belhadj et al. [45] at 313.15 K, □, Belhadj et al. [45] at 323.15 K; (b) 2-(2-ethoxyethoxy)ethanol (1) + 2-propanol (2): Experimental data in this work: (●), at 293.15 K, (◆), at 303.15 K, (▲), at 313.15 K, (■), at 323.15 K; o, Ouaar et al. [47] at 293.15 K, ◇, Ouaar et al. [47] at 303.15 K, Δ, Ouaar et al. [47] at 313.15 K, □, Ouaar et al. [47] at 323.15 K; (c) 2-methoxyethanol (1) + 2-propanol (2): Experimental data in this work: (●), at 293.15 K, (◆), at 303.15 K, (▲), at 313.15 K, (■), at 323.15 K; (d) 2-phenoxyethanol (1) + 2-propanol (2): Experimental data in this work: (●), at 293.15 K, (◆), at 303.15 K, (▲), at 313.15 K, (■), at 323.15 K; o, Makhlouf et al. [14] at 293.15 K, ◇, Makhlouf et al. [14] at 303.15 K, Δ, Makhlouf et al. [14] at 313.15 K, □, Makhlouf et al. [14] at 323.15 K; (e) 2-buthoxyethanol (1) + 2-propanol: Experimental data in this work: (●), at 293.15 K, (◆), at 303.15 K, (▲), at 313.15 K, (■), at 323.15 K; o, Dubey et al. [49] at 293.15 K, ◇, Dubey et al. [49] at 303.15 K, Δ, Dubey et al. [49] at 313.15 K. (——), calculated values of refractive index with the polynomial equation (Eq. 21)

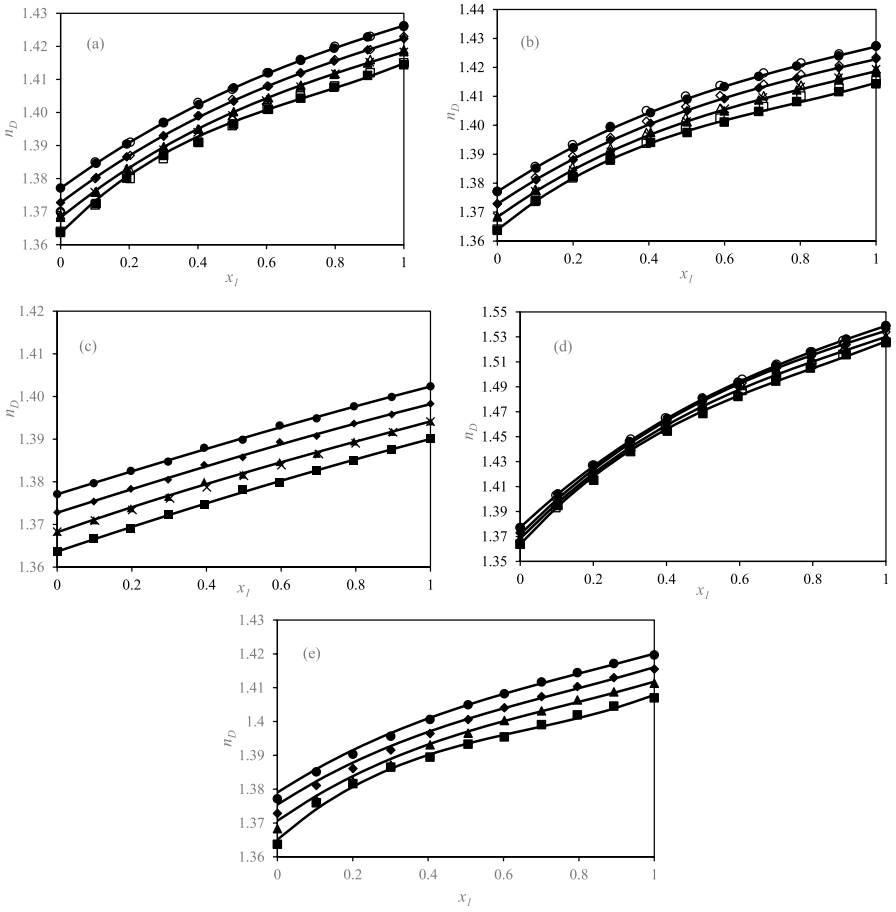

Fig. 5 Experimental values of refractive index, n_D, as a function of mole fraction of x_1 for binary mixtures: (a) 2-(2-methoxyethoxy)ethanol (1) + 2-propanol (2): Experimental data in this work: (●), at 293.15 K, (◆), at 303.15 K, (▲), at 313.15 K, (■), at 323.15 K; o, Belhadj et al. [45] at 293.15 K, ◊, Belhadj et al. [45] at 303.15 K, Δ, Belhadj et al. [45] at 313.15 K, +, Abala et al. [46] at 313.15 K, □, Belhadj et al. [45] at 323.15 K; (b) 2-(2-ethoxyethoxy)ethanol (1) + 2-propanol (2): Experimental data in this work: (●), at 293.15 K, (◆), at 303.15 K, (▲), at 313.15 K, (■), at 323.15 K; o, Ouaar et al. [47] at 293.15 K, ◊, Ouaar et al. [47] at 303.15 K, Δ, Ouaar et al. [47] at 313.15 K, +, Abala et al. [46] at 313.15 K, □, Ouaar et al. [47] at 323.15 K; (c) 2-methoxyethanol (1) + 2-propanol (2): Experimental data in this work: (●), at 293.15 K, (◆), at 303.15 K, (▲), at 313.15 K, (■), at 323.15 K; +, Abala et al. [46] at 313.15 K; (d) 2-phenoxyethanol (1) + 2-propanol (2): Experimental data in this work: (●), at 293.15 K, (◆), at 303.15 K, (▲), at 313.15 K, (■), at 323.15 K; o, Makhlouf et al. [14] at 293.15 K, ◊, Makhlouf et al. [14] at 303.15 K, Δ, Makhlouf et al. [14] at 313.15 K, □, Makhlouf et al. [14] at 323.15 K; (e) 2-buthoxyethanol (1) + 2-propanol: Experimental data in this work: (●), at 293.15 K, (◆), at 303.15 K, (▲), at 313.15 K, (■), at 323.15 K. (——), calculated values of refractive index with the polynomial equation (Eq. 21)

For the speed of sound, 2-PrOH exhibited AADs of 0.03 % at 293.15 K (with Ouaar et al. [47]) and 0.12 % at 293.15 K (with Belhadj et al. [45]). 22MEE showed an AAD of 0.25 % at 323.15 K (with Belhadj et al. [45]). For 22EEE, the AAD ranged from 0.09 % at 293.15 K to a maximum of 0.12 % at 323.15 K (with Ouaar et al. [47]). The 2PhE also demonstrated good consistency, with an AAD of 0.03 % at 293.15 K (with Makhlouf et al. [14]). However, no literature data were found for 2ME and 2BE.

Moreover, the low AAD confirms the reliability of our experimental data for refractive index. For 2-PrOH, an AAD of 0.15 % was found at 313.15 K (with Abala et al. [46]). At 293.15 K, good agreement was also found for 22MEE with an AAD of 0.04 % for 22MEE (with Belhadj et al. [45]), 0.006 % for 22EEE (with Ouaar et al. [47]). For 2ME an AAD of 0.005 % was found at 293.15 K (with Lifi et al. [12]), and 0.15 % at 303.15 K (with Jeevanandham et al. [50]). For 2PhE an AAD of 0.02 % was showed at 293.15 K (with Makhlouf et al. [14]). The 2BE showed an AAD of 0.10 % at 303.15 K (with Jeevanandham et al. [50]).

6.2.4.2 For Binary Mixtures Experimental data for all binary mixtures studied in the present work were compared with data previously published by Makhlouf et al. [14], Belhadj et al. [45], Abala et al. [46], Ouaar et al. [47], Zarei et al. [48], and Dubey et al. [49]. The average absolute deviations (AADs) for density for the binary mixtures studied over the temperature range 293.15 K to 323.15 K indicate excellent agreement with literature data. For the 22MEE + 2-PrOH mixture, the smallest AADs was 0.04 % at 313.15 K and the highest reached 0.13 % at 323.15 K (with Belhadj et al. [45]). The 22EEE + 2-PrOH system also showed low deviations, with an AAD of 0.01 % at 313.15 K and 0.07 % at 323.15 K (with Ouaar et al. [47]). For the 2ME + 2-PrOH mixture, deviations were particularly low, ranging from 0.007 % at 313.15 K to 0.51 % at 293.15 K (with Zarei et al. [48]). The 2PhE + 2-PrOH system exhibited small AADs between 0.02 % (at 293.15 K, 303.15 K, and 313.15 K) and 0.03 % at 323.15 K, confirming strong reliability of the experimental measurements (with Makhlouf et al. [14]). In contrast, the 2BE + 2-PrOH mixture presented the highest AADs among the studied systems, reaching up to 0.17 % at 303.15 K (with Dubey et al. [49]).

For speed of sound, the mixtures also showed very good agreement with literature values across the studied temperature range. The 22MEE + 2-PrOH mixture showed deviations between 0.05 % at 293.15 K and 0.32 % at 323.15 K (with Belhadj et al. [45]). The 22EEE + 2-PrOH system presented similarly low AADs ranging from 0.03 % at 293.15 K to 0.06 % at 323.15 K (with Ouaar et al. [47]). The 2PhE + 2-PrOH system had AADs from 0.01 % at 293.15 and 323.15 K to 0.27 % at 303.15 K, confirming good agreement (with Makhlouf et al. [14]). However, the 2BE + 2-PrOH mixture exhibited significantly good AAD, with values of 0.01 % at 313.15 K (with Dubey et al. [49]). No data was found the binary 2ME + 2-PrOH in the literature.

Refractive index measurements demonstrated high accuracy across all systems. For the 22MEE + 2-PrOH mixture, AADs ranged from 0.005 % at 303.15 K to 0.01 % at 313.15 K, confirming reliable results (with Belhadj et al. [45]). The 22EEE + 2-PrOH mixture showed also low deviations, 0.004 % at 293.15 K and

0.04 % at 313.15 K (with Ouaar et al. [47]). For the 2ME + 2-PrOH system, the AAD was 0.02 % at 313.15 (with Abala et al. [46]). The 2PhE + 2-PrOH mixture exhibited excellent consistency, with AADs from 0.001 % at 303.15 K to 0.07 % at 323.15 K (with Makhlouf et al. [14]). No data was found for the binary 2BE + 2-PrOH in the literature.

6.3 Derivative Properties

The derivative properties such as isothermal compressibility, excess molar volume and deviation in refractive index of binary mixtures of: x 22MEE + $(1 - x)$ 2-PrOH; x 22EEE + $(1 - x)$ 2-PrOH; x 2ME + $(1 - x)$ 2-PrOH; x 2PhE + $(1 - x)$ 2-PrOH and x 2BE + $(1 - x)$ 2-PrOH, were fitted along the 4 temperatures (293.15 K, 303.15 K, 313.15 K and 323.15 K) under atmospheric pressure (0.1 MPa). The A_i parameters values used to adjust k_s, V^E, and $\Delta\, n_D$ of each studied binary using Eq. 20 are listed in Table S5.

6.3.1 Isothermal Compressibility (k_s)

Across all systems, k_s exhibits a non-linear dependency on composition, as shown in Fig. 6, which is typical of mixtures where significant molecular interactions occur. In many cases, a minimum in compressibility appears at intermediate mole fractions, implying stronger interactions such as hydrogen bonding or specific association between the alcohol and ether molecules. This reduction in compressibility indicates decreased molecular free volume and enhanced structural packing.

As temperature increases, a general rise in compressibility is observed. This behavior is expected since elevated temperatures weaken intermolecular interactions and increase the average molecular spacing, leading to greater compressibility. The results values are well-represented by the polynomial correlation, as seen from the close alignment between the data points and the fitted curves. This agreement validates the use of the empirical model in describing the k_s behavior over the investigated range of temperatures and compositions.

6.3.2 Excess Molar Volume (V^E)

The excess molar volume (V^E) behavior (Fig. 7) of binary mixtures containing glycol ethers and 2-PrOH varies notably with both composition and temperature, reflecting differences in molecular interactions and structural compatibility between the components. Among the studied systems, the mixture of 2ME with 2-PrOH displays a unique trend: at 293.15 K and 303.15 K, positive V^E values are observed, suggesting volume expansion due to the disruption of self-association (mainly hydrogen bonding) in the pure components. At 313.15 K, however, the system shows negative V^E values, likely due to the formation of stronger hetero-interactions, which result in closer molecular packing and contraction. When the temperature increases further to 323.15 K, V^E becomes positive again, indicating

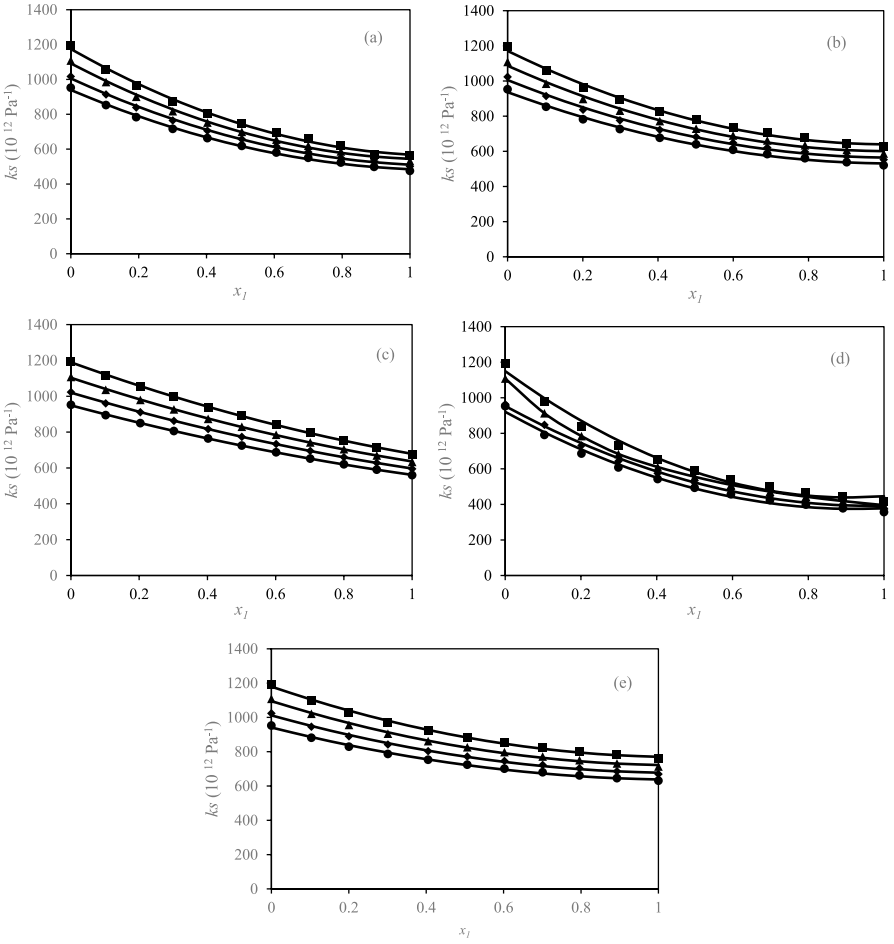

Fig. 6 Calculated values of isentropic compressibility, κ_S, as a function of mole fraction of x_1 for binary mixtures: (a) 2-(2-methoxyethoxy)ethanol + 2-propanol; (b) 2-(2-ethoxyethoxy)ethanol + 2-propanol; (c) 2-methoxyethanol + 2-propanol; (d) 2-phenoxyethanol + 2-propanol and (e) 2-buthoxyethanol + 2-propanol. where: ●, 293.15 K; ◆, 303.1 K; ▲, 313.15 K; ■, 323.15 K. (solid line) Calculated values of isentropic compressibility with the polynomial equation (Eq. 21)

that the thermal weakening of intermolecular forces reduces packing efficiency and leads to expansion upon mixing.

In contrast, the mixtures of 22MEE, 22EEE, 2PhE, and 2BE with 2-PrOH consistently exhibit negative excess molar volumes across all compositions and temperatures. This contraction upon mixing can be attributed to strong associative interactions especially hydrogen bonding and dipole–dipole interactions between dissimilar molecules, which promote a more efficient and compact molecular arrangement.

The shape of the V^E curves is generally smooth and symmetric, with minima occurring near the equimolar composition ($x_1 \approx 0.5$), suggesting a balanced

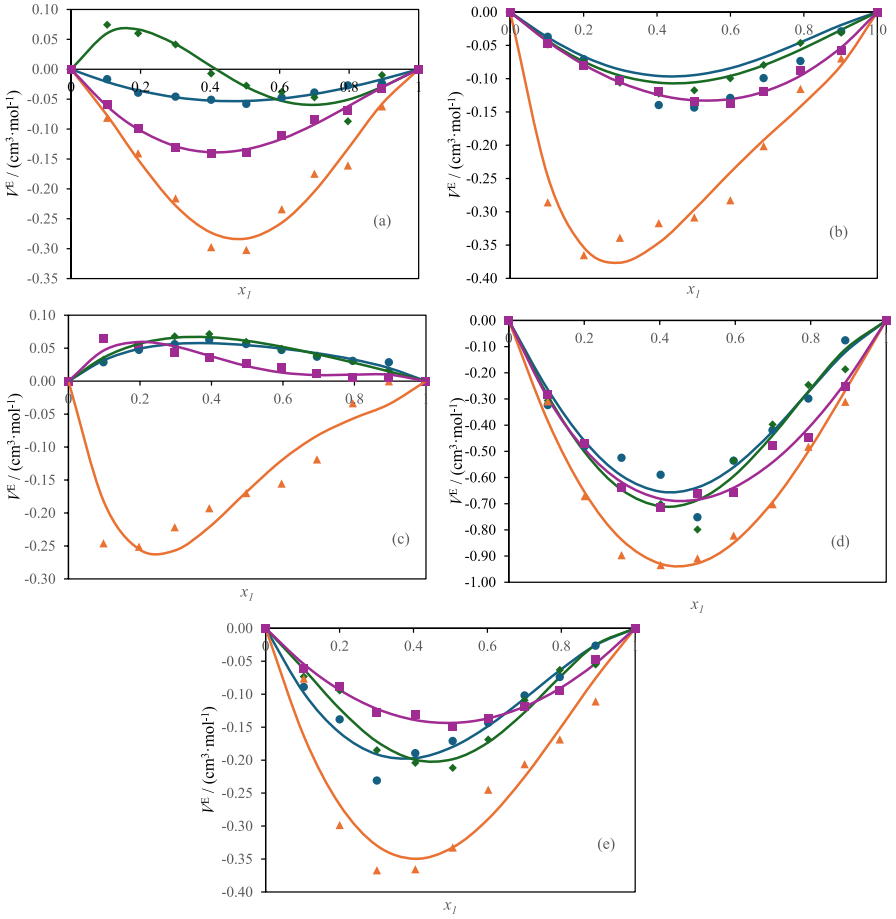

Fig. 7 Tendency curves of calculated values of excess molar volumes for the mixtures: (a)×2-(2-methoxyethoxy) ethanol + (1 − x) 2-propanol; (b)×2-(2-ethoxyethoxy) ethanol + (1 − x) 2-propanol; (c)×2-methoxyethanol + (1 − x) 2-propanol; (d)×2-phenoxyethanol + (1 − x) 2-propanol; (e)×2-butoxyethanol + (1 − x) 2-propanol as a function of the mole fraction, where: ●, 293.15 K; ◆, 303.15 K; ▲, 313.15 K; ■, 323.15 K. Calculated values of excess volume with the Redlich–Kister equation (Eq. 20) are presented by solid lines (—)

contribution from both components in most cases. However, slight asymmetry is observed in mixtures involving structurally complex molecules, where differences in molecular size, shape, and interaction strength influence the volumetric behavior. Across all systems, temperature plays a crucial role: increasing it typically reduces the magnitude of contraction or expansion, highlighting the sensitivity of intermolecular interactions to thermal energy. These observations underscore how variations in molecular architecture and interaction types significantly affect the mixing behavior and excess molar volume characteristics of glycol ether–alcohol mixtures.

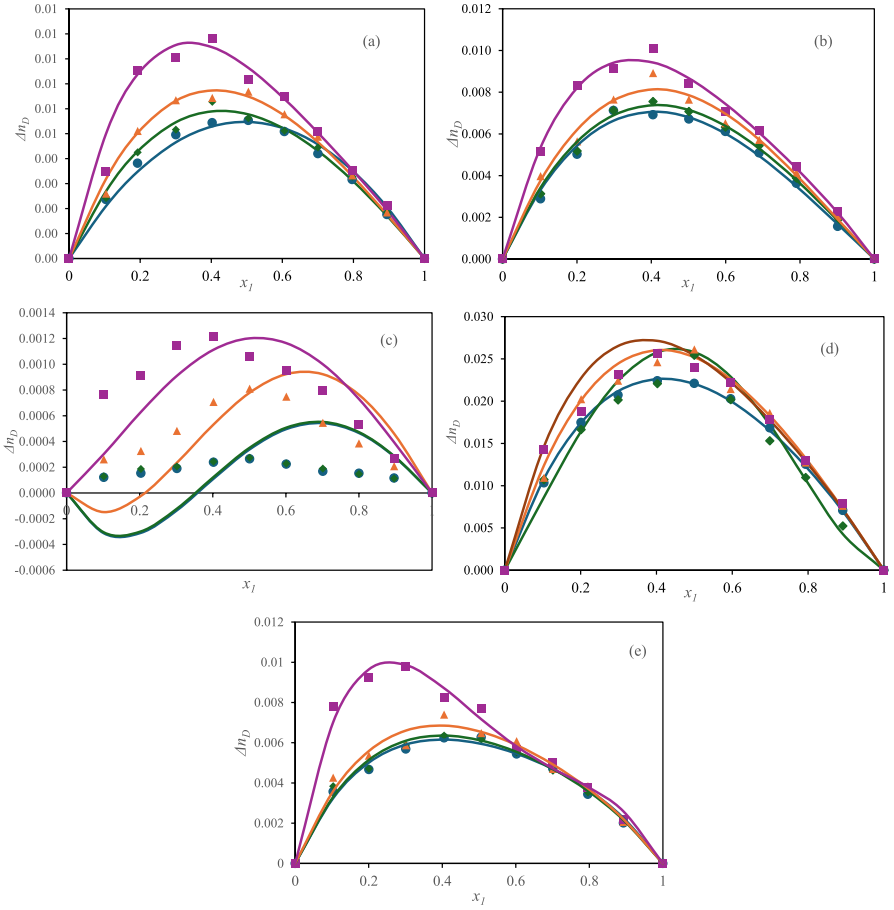

Fig. 8 Calculated values of Δn_D as a function of x_1 for: (a) 2-(2-methoxyethoxy)ethanol (1) + 2-propanol (2); (b) 2-(2-ethoxyethoxy)ethanol (1) + 2-propanol (2); and (c) 2-methoxyethanol (1) + 2-propanol (2); (d) 2-phenoxyethanol (1) + 2-propanol (2); (e) 2-buthoxyethanol (1) + 2-propanol. At temperatures: ●, 293.15 K; ◆, 303.15 K; ▲, 313.15 K; ■, 323.15 K. Calculated values of Δn_D with Eq. 20: (——), at 293.15 K, (——), at 303.15 K, (——), at 313.15 K and (——), at 323.15 K

6.3.3 Deviation in Refractive Index, (Δn_D)

The refractive index deviation (Δn_D) for the binary mixtures of oxygen additive with 2-PrOH, was determined using the following expression:

$$\Delta n_D = n_D - \sum_{i+1}^{N} x_i n_{Di} \tag{24}$$

where n_D represents the measured refractive index of the mixture, x_i is the mole fraction of component i, and n_{Di} is the refractive index of the pure component. The variations of Δn_D as a function of composition are illustrated in Fig. 8 at 293.15, 303.15,

313.15 and 323.15 for all the mixtures. The calculated values across the five binary mixtures demonstrate clear temperature-dependent behavior, with the excess property generally increasing with temperature at most compositions. For all systems, the maximum deviation tends to occur near equimolar compositions, reflecting strong non-ideal interactions between 2-PrOH and each glycol ether. Among the mixtures, those containing longer alkyl chains, such as 2BE and 22EEE, show broader and higher peaks in the excess property, indicating stronger disruption of self-association and more significant structural dissimilarity between the components. In contrast, mixtures with shorter or more polar molecules like 2-ME or 22MEE display narrower curves, suggesting a more moderate deviation from ideality. The temperature effect is especially noticeable in mixtures with 2-PhE, where the asymmetry and potential for both hydrophobic and polar interactions lead to greater sensitivity. Overall, the model used to generate these curves successfully captures the key trends observed experimentally, including the influence of molecular size, polarity, and hydrogen bonding potential, making it a reliable approach for describing such complex mixtures.

7 Conclusions

This work investigated the thermodynamic behavior of binary mixtures composed of 2-propanol and various glycol ethers at various temperatures. Experimental measurements of density, speed of sound, refractive index, and excess molar enthalpy enabled the determination of key excess properties, including excess molar volume and refractive index deviation. These properties were correlated using the R–K equation and a polynomial equation to describe their variation with composition. Density data were treated both through empirical polynomial fitting and predictive modeling using the PC-SAFT and Peng–Robinson equations of state. In addition to R–K correlation, the excess molar enthalpy was analyzed using thermodynamic models UNIQUAC, NRTL, and UNIFAC to gain insight into molecular-level interactions. The integration of experimental results with both empirical and theoretical methods provides a consistent framework for understanding non-ideal behavior in such systems, supporting their potential application in renewable fuel and solvent technologies.

Supplementary Information The online version contains supplementary material available at https://doi.org/10.1007/s10765-025-03616-3.

Author Contributions K.S. wrote the main manuscript text, software, investigation, formal analysis; M.L. reviewed the manuscript, software, investigation, methodology, formal analysis; I.A. investigation, formal analysis; N.M.R. supervision, validation; F.E.M.A. reviewed the manuscript, supervision, validation; F.A. supervision, validation.

Funding Open access funding provided by FEDER European Funds and the Junta de Castilla y León under the Research and Innovation Strategy for Smart Specialization (RIS3) of Castilla y León 2021-2027. Open access funding provided by UNIVERSIDAD DE BURGOS.

Data Availability No datasets were generated or analysed during the current study.

Declarations

Competing Interests The authors declare no competing interests.

References

1. M.Y. Raza, W. Wang, Q. Javed, Energy Strategy Rev. **59**, 101750 (2025)
2. S. Yarramsetti, M. Girirajan, S. Kalluri, S. Sangaraju, P.S. Maram, Mater. Chem. Phys. **320**, 129424 (2024)
3. M.H. Khademi, M. Lotfi-Varnoosfaderani, Fuel **310**, 122359 (2022)
4. Y. Marcus, J. Chem. Soc. Faraday Trans. **87**, 2995 (1991)
5. P. Luo, C. Yang, Y. Gu, Fluid Phase Equilib. **252**, 143 (2007)
6. F. Zhou, R. Yan, G. Li, W. Han, Renew. Energy **235**, 121374 (2024)
7. J. Motte, P. Nachtergaele, M. Mahmoud, H. Vleeming, J.W. Thybaut, J. Poissonnier, J. Dewulf, J. Clean. Prod. **379**, 134843 (2022)
8. M. Lifi, N. Muñoz-Rujas, G. Rubio-Pérez, F. Aguilar, F.E. M'hamdiAlaoui, J. Chem. Eng. Data **69**, 2554 (2024)
9. M. Lifi, J.-P. Bazile, J.-L. Daridon, E.A. Montero, F. Aguilar, N. Muñoz-Rujas, J. Chem. Thermodyn. **206**, 107476 (2025)
10. M. Lifi, G. Rubio-Pérez, H. Lifi, N. Muñoz-Rujas, F. Aguilar, F.E.M. Alaoui, J. Chem. Thermodyn. **177**, 106933 (2023)
11. S. Ganji, T.S. Krishna, D. Venkatesan, R. Day, D. Ramachandran, J. Chem. Thermodyn. **201**, 107396 (2025)
12. M. Lifi, I. Abala, N. Munoz-Rujas, F. Aguilar, E.A. Montero, L. Negadi, F.E. M'hamdiAlaoui, J. Chem. Thermodyn. **164**, 106593 (2022)
13. V. Alonso, M. García, J.A. González, I. García De La Fuente, J.C. Cobos, Thermochim. Acta **521**, 107 (2011)
14. H. Makhlouf, N. Muñoz-Rujas, F. Aguilar, B. Belhachemi, E.A. Montero, I. Bahadur, L. Negadi, J. Chem. Thermodyn. **128**, 394 (2019)
15. C.M. Kinart, M. Maj, A. Ćwiklińska, W.J. Kinart, J. Mol. Liq. **139**, 1 (2008)
16. N. Chaudhary, A. Kumar Nain, J. Mol. Liq. **346**, 117923 (2022)
17. A.M. Mainar, S.M. García-Abarrio, A.M.F. Palavra, J.S. Urieta, J.I. Pardo, J. Chem. Eng. Data **56**, 3818 (2011)
18. O. Redlich, A.T. Kister, Ind. Eng. Chem. **40**, 345 (1948)
19. D.S. Abrams, J.M. Prausnitz, AIChE J. **21**, 116 (1975)
20. U. Weidlich, J. Gmehling, Ind. Eng. Chem. Res. **26**, 1372 (1987)
21. M.M. Abbott, H.C. Van Ness, AIChE J. **21**, 62 (1975)
22. J. Gross, G. Sadowski, Ind. Eng. Chem. Res. **40**, 1244 (2001)
23. F. Aguilar, F.E.M. Alaoui, C. Alonso-Tristán, J.J. Segovia, M.A. Villamañán, E.A. Montero, J. Chem. Eng. Data **54**, 1672 (2009)
24. European co-operation for Accreditation, EA 4/02: *Expression of the Uncertainty of Measurement in Calibration*, December (1999)
25. J. Gmehling, J. Li, M. Schiller, Ind. Eng. Chem. Res. **32**, 178 (1993)

26. J. Gross, G. Sadowski, Ind. Eng. Chem. Res. **41**, 5510 (2002)
27. I. Abala, F.E.M. Alaoui, A. Sahib Eddine, F. Aguilar, N.M. Rujas, E. Montero, J. Chem. Eng. Data **64**, 3861 (2019)
28. I. Abala, M. Lorenzo-Bañuelos, H. Lifi, M. Lifi, N. Muñoz-Rujas, F. Aguilar, F.E. M'hamdiAlaoui, J. Chem. Eng. Data **67**, 3532 (2022)
29. I. Abala, M. Lifi, Y. Chhiti, R. A. Belale, F. E. M. Alaoui, M. E. Khouakhi, and L. Deshayes, in *2020 5th international conference on renewable energy for developing countries REDEC* (IEEE, Marrakech, 2020), pp. 1–6.
30. C.L. Yaws, Critical Properties and Acentric Factor—Organic Compounds, in: Thermophysical Properties of Chemicals and Hydrocarbons, (Elsevier, Amsterdam, 2014)
31. M. Škerget, Z. Novak-Pintarič, Ž Knez, Z. Kravanja, Fluid Phase Equilib. **203**, 111 (2002)
32. H. Renon, J.M. Prausnitz, AIChE J. **14**, 135 (1968)
33. P.R. Bevington, D.K. Robinson, *Data Reduction and Error Analysis for the Physical Sciences* (WCD/McGraw-Hill, Boston, 1992)
34. A. Fredenslund, *Vapor-Liquid Equilibria Using Unifac: A Group-Contribution Method* (Elsevier, Amsterdam, 2012)
35. B.E. Poling, J.M. Prausnitz, J.P. O'Connell, *Properties of Gases and Liquids*, 5th edn. (McGraw-Hill Education, New York, 2020)
36. M. Lifi, I. Abala, R. Briones-Llorente, N. Muñoz-Rujas, F. Aguilar, F.E. M'hamdiAlaoui, J. Chem. Eng. Data **68**, 3062 (2023)
37. K. Kumar, B.K. Nandi, V.K. Saxena, R. Kumar, Alex. Eng. J. **106**, 411 (2024)
38. A.S. Buchelnikov, V.P. Evstigneev, M.P. Evstigneev, Phys. Chem. Chem. Phys. **21**, 7717 (2019)
39. G.P. Dubey, R. Singh, J. Chem. Thermodyn. **197**, 107337 (2024)
40. M. Lifi, J. Lorenzo, F. Aguilar, N. Muñoz-Rujas, E.A. Montero, Y. Chhiti, F.E.M. Alaoui, J. Chem. Thermodyn. **153**, 106306 (2021)
41. N.-N. Wang, Q.-Z. Li, Z.-W. Yu, Appl. Spectrosc. **63**, 1356 (2009)
42. A. Nowok, M. Dulski, J. Grelska, A.Z. Szeremeta, K. Jurkiewicz, K. Grzybowska, M. Musiał, S. Pawlus, J. Phys. Chem. Lett. **12**, 2142 (2021)
43. C. Medcraft, S. Zinn, M. Schnell, A. Poblotzki, J. Altnöder, M. Heger, M.A. Suhm, D. Bernhard, A. Stamm, F. Dietrich, M. Gerhards, Phys. Chem. Chem. Phys. **18**, 25975 (2016)
44. R.L. Brinkley, R.B. Gupta, Ind. Eng. Chem. Res. **37**, 4823 (1998)
45. D. Belhadj, I. Bahadur, A. Negadi, N. Muñoz-Rujas, E. Montero, L. Negadi, J. Chem. Eng. Data **65**, 5192 (2020)
46. I. Abala, M. Lifi, R. Briones-Llorente, H. Lifi, F. Aguilar, and F. E. M'hamdi Alaoui, J. Chem. Eng. Data (2025)
47. F. Ouaar, I. Mokbel, A. Negadi, F. Aguilar, E.A. Montero, J. Jose, I. Bahadur, L. Negadi, J. Chem. Eng. Data **65**, 2351 (2020)
48. H.A. Zarei, F. Jalili, J. Chem. Thermodyn. **39**, 55 (2007)
49. G.P. Dubey, P. Kaur, Fluid Phase Equilib. **354**, 114 (2013)
50. P. Jeevanandham, S. Kumar, P. Periyasamy, J. Mol. Liq. **188**, 203 (2013)

Authors and Affiliations

Khaoula Samadi[1,4] · Mohamed Lifi[2] · Ilham Abala[3] · Natalia Muñoz-Rujas[4] · Fatima Ezzahrae M'hamdi Alaoui[1] · Fernando Aguilar[4]

✉ Mohamed Lifi
mlifi@ubu.es

[1] Energy Laboratory, Faculty of Sciences, University of Abdelmalek Essaadi, Tetouan, Morocco

[2] Department of Mathematics and Computing, Faculty of Science, University of Burgos, 09001 Burgos, Spain

[3] Laboratory of Catalysis and Corrosion of Materials (LCCM), Chemistry Department, Chouaïb Doukkali University, B.P. 24000, El Jadida, Morocco

[4] Departamento de Ingeniería Electromecánica, Escuela Politécnica Superior, Universidad de Burgos, 09006 Burgos, Spain